Universidade de Lisboa
Faculdade de Ciências
Departamento de Física

Scan path optimization for active beam delivery in charged particle therapy

Marta Filipa Ferraz Dias

DISSERTAÇÃO

MESTRADO INTEGRADO EM ENGENHARIA BIOMÉDICA E BIOFÍSICA

PERFIL EM RADIAÇÕES EM DIAGNÓSTICO E TERAPIA

2012

Universidade de Lisboa
Faculdade de Ciências
Departamento de Física

Scan path optimization for active beam delivery in charged particle therapy

Marta Filipa Ferraz Dias

Dissertação orientada por Professor Doutor Marco Riboldi e Professor Doutor Luís Peralta

MESTRADO INTEGRADO EM ENGENHARIA BIOMÉDICA E BIOFÍSICA

PERFIL EM RADIAÇÕES EM DIAGNÓSTICO E TERAPIA

2012

Para ti, Mãe. Para ti, Pai. E para ti, Marta do futuro

Acknowledgments

First of all, I would like to express the deepest appreciation to both my supervisors Professor Marco Riboldi and Professor Luís Peralta. To Professor Marco Riboldi for offering me the opportunity to work with him, for helping me in my PhD application and for sharing with me his knowledge and patience. To Professor Luís Peralta for being not only a professor but a friend, and for all the shared support and knowledge during my academic life.

In addition, I would like to thank Professor João Seco and professor Eduardo Ducla-Soares. Professor João Seco provided the first contact with Professor Marco Riboldi, and was always supportive and encouraging during the development of this thesis. Professor Eduardo Ducla-Soares, for being a mentor and a friend during my academic life. Even not being my supervisor, always supported me and showed interested in my work. I deeply believe I would not have reach so far without his help.

I gratefully acknowledge the financial support from the LLP/Erasmus Grant.

I would like to thank a todos aqueles que falam esta língua maravilhosa, certamente que de alguma forma contribuiram para eu ter chegado tão longe. Um agradecimento especial à Maria Rodrigues e Diana Rosa - *Se vivia sem elas?! Vivia, mas não era a mesma coisa...* - à Débora Salvado e ao Nuno da Silva por se mostrarem sempre disponíveis para ajudar e ao Rafael Henriques por toda a sua amizade, paciência e atenção.

Finalmente, à minha família. Às minhas irmãs por me fazerem sentir sempre bem-vinda a casa, mesmo quando me "melgam". E em especial aos meus pais a quem devo praticamente tudo o que consegui alcançar. Muito obrigada...

Resumo

De acordo com a Organização Mundial de Saúde, o cancro é uma das principais causas de morte em todo o mundo com certa de 7.6 milhões de mortes em 2008. Excluindo o cancro de pele não-melanoma foi estimado que cerca de 45% dos pacientes com cancro, se tratados, podem ser curados. Existem diferentes métodos de tratamento para o cancro sendo a cirurgia, quimioterapia e radioterapia os tratamentos padrão. A radioterapia possui um importante papel como método de tratamento do cancro, apresentando uma taxa de cura de cerca de 23% (12% se utilizada sozinha e 11% quando combinada com cirurgia ou quimioterapia). Atualmente a técnica de radioterapia dominante, conhecida como "convencional", utiliza fotões. Contudo, o interesse na utilização de aceleradores de partículas carregadas (considerando apenas partículas com massas iguais ou superiores à do protão) tem vindo a aumentar consideravelmente. Esse interesse deve-se principalmente ao facto de este tipo de partículas possuir uma curva de distribuição de dose em profundidade que apresenta um máximo ao qual se dá o nome de pico de Bragg. Antes do pico de Bragg a deposição de energia é praticamente constante, sendo que após este, decai bruscamente. Tendo em conta esta distribuição, Wilson propôs o uso de protões como técnica de alta precisão do tratamento do cancro. A terapia do cancro com partículas carregadas (protões e iões de carbono) tem vindo a mostrar um grande crescimento, sendo que atualmente já existem cerca de 38 centros no mundo onde esta técnica é utilizada. Um dos primeiros centros totalmente dedicado ao uso de partículas carregadas no tratamento do cancro é o Centro Nazionale di Adroterapia Oncologica (CNAO), que se situa em Itália. Neste centro é utilizada uma técnica de irradiação de tumores denominada de active scanning technique. Neste método, o tumor é dividido em "fatias" a diferentes profundidades. Em cada "fatia" é definido um conjunto de pontos que necessitam de ser irradiados de forma a obter-se, no final, uma distribuição de dose uniforme no tumor. A irradiação de cada "fatia" pode ser feita utilizando duas técnicas diferentes: o discrete scanning e o quadiscrete scanning. Na técnica de discrete scanning, o feixe de irradiação é guiado ao longo da "fatia" irradiando os pontos anteriormente definidos, sendo desligado durante a transição de pontos consecutivos. Na técnica de quasidiscrete scanning o feixe não é desligado nessas transições, levando à irradiação desnecessária das áreas onde não se encontram pontos de irradiação. Esta irradiação desnecessária, leva à deposição de uma dose extra no tumor, que senão for tida em conta pode influenciar a distribuição de dose final do tumor. Desta forma, uma optimização do caminho feito pelo feixe, pode levar a uma diminuição da dose extra. Adicionalmente, em ambas as técnicas (discrete e quasidiscrete scanning) uma optimização do caminho poderá também levar a uma diminuição do tempo de irradiação e da energia utilizada pelo equipamento. O principal objetivo desta tese foi estudar o efeito da optimização do caminho feito pelo feixe em planos de tratamento de pacientes do CNAO. Foram definidos os seguintes objetivos secundários:

- Identificação de possíveis estratégias para resolução do problema proposto através do estudo da literatura corrente sobre algoritmos de optimização;

- Implementação e avaliação da performance das estratégias identificadas, utilizando planos de tratamento de pacientes do CNAO;
- Avaliação do efeito clínico da utilização dos métodos propostos;
- Desenvolvimento de uma ferramenta capaz de optimizar o caminho percorrido pelo feixe, utilizando os métodos de optimização identificados.

Esta tese encontra-se dividida em cinco capítulos. No primeiro capítulo foram introduzidos alguns conceitos sobre terapia do cancro com partículas carregadas e algoritmos de optimização. No capítulo 2 foi explicada a abordagem tomada para a resolução do problema e quais os métodos utilizados. Os resultados obtidos para os métodos propostos encontram-se no capítulo 3. Finalmente no capítulo 4 e 5 é apresentada a discussão dos resultados e as conclusões obtidas. De forma a cumprir os objetivos propostos, foram identificados dois principais algoritmos de optimização: Simulated Annealing (SA) e Algoritmos Genéticos (GAs). O SA foi anteriormente proposto por Pardo e Kang como uma possível solução para o problema identificado. Este algoritmo é baseado no processo de annealing para formação de cristais. Enquanto que os algoritmos genéticos baseiam-se no principio da sobrevivência dos mais fortes introduzido por Darwin. Tal como este principio, os GA podem ser divididos em três partes: seleção, crossover ou reprodução e mutação. Neste trabalho foram testados diferentes métodos de crossover e mutação, sendo que o método que ofereceu melhores resultados (uma convergência mais rápida para uma "boa" solução) foi um algoritmo genético híbrido - Hybrid Genetic Algorithm with Heuristics (HyGA). O HyGA e o SA foram utilizados para optimização dos caminhos feitos pelo feixe de irradiação em 10 planos de tratamento de pacientes do CNAO. Em comparação com o HyGA, o SA apresentou em média, caminhos mais longos para "fatias" com pequenas quantidades de pontos de irradiação e para "fatias" onde estes se encontravam distribuídos de forma não uniforme. Contudo, os dois algoritmos obtiveram caminhos mais curtos que o sistema de planeamento do CNAO (CNAO's TPS). Estes algoritmos também evitaram a presença de interseções nos seus caminhos e a irradiação de áreas onde não existiam pontos de irradiação. De forma a evitar a irradiação de áreas onde não existem pontos de irradiação, no CNAO é utilizado um equipamento (o chopper), que deflecte o feixe na zona de extração, evitando a irradiação da "fatia". No CNAO, o chopper é utilizado quando a distÃ¢ncia entre pontos consecutivos é maior que 2 cm. Tendo em conta a existência do chopper, o HyGA foi implementado com um método de clustering. Este método agrupa os pontos de irradiação numa "fatia" em diferentes grupos (clusters) e optimiza o caminho percorrido pelo feixe em cada grupo de forma independente. Neste método o chopper foi utilizado quando ocorresse uma transição entre clusters. As implicações clinicas dos métodos propostos (SA e HyGA) foram avaliadas tendo em conta o número de partículas entregues, o número de partículas desperdiçadas devido ao uso do chopper e o número de vezes que este foi utilizado. O estudo do número de partículas entregues foi feito recorrendo a um pencil beam algorithm. Relativamente ao número de partículas entregues,

o SA e o HyGA, apesar de apresentarem caminhos mais curtos, não reduziram o número de partículas entregues nos caminhos calculados com o CNAO's TPS. Contudo, o mesmo não foi verificado para o HyGA com clustering, que obteve uma redução de cerca de 2%. Uma das implicações da utilização do chopper é um aumento no número de partículas desperdiçadas pelo equipamento. O HyGA e o SA obtiveram uma redução média de 86% e 93% no número de partículas desperdiçadas com o CNAO's TPS, enquanto que com o HyGA com clustering foi registado um aumento médio de cerca de 41%. Tendo em conta os resultados obtidos, foi possível concluir que os algoritmos de optimização propostos poderão ser úteis para duas diferentes finalidades. A primeira é na redução da energia gasta pelo equipamento. No CNAO, isto pode ser alcançado utilizando os algoritmos SA e o HyGA, pois irão reduzir o número de partículas desperdiçadas. Enquanto que para centros onde o chopper não seja utilizado, estes algoritmos obterão caminhos mais curtos levando a uma redução no funcionamento do equipamento. A segunda finalidade é na redução na dose extra no paciente, que pode ser reduzida no CNAO utilizando o HyGA com clustering. Noutros centros esta redução será devida ao encurtamento dos caminhos percorridos pelo feixe de irradiação. Visto que cada um dos diferentes métodos de optimização apresenta desvantagens e vantagens, foi desenvolvida uma ferramenta que oferece a possibilidade do cálculo individual de cada "fatia" utilizando os diferentes algoritmos de optimização: SA, HyGA, HyGA com clustering e CNAO's TPS. Em suma, como trabalho futuro deverá ser estudado o efeito que a dose extra, entregue pelos algoritmos SA e HyGA, terá num paciente.

Palavras Chave: Optimizaçao dos caminhos, Algoritmos, fatia, pontos de irradiação.

Abstract

The CNAO (Centro Nazionale di Adroterapia Oncologica) performs charged particle therapy with an active scanning technique called *quasidiscrete scanning*. In active scanning the target volume is divided into isoenergy slices in which a set of irradiation spots is defined. The irradiation beam is then steered through the slice, delivering the number of particles prescribed to each spot. The beam is never turned off during the transition between irradiation spots, which leads to an extra dose of radiation delivered during these transitions. Optimization of the scan path for each slice is crucial for a reduction in the transit dose. The main aim of this work was to study the performance and the clinical implications of different optimization algorithms in ten real treatment plans from CNAO patients. The optimization algorithms used are Simulated Annealing and Genetic Algorithms. The performances of different genetic algorithm methods were studied, leading to the selection of the Hybrid Genetic Algorithm with Heuristics (HyGA). The SA and HyGA produced on average shorter paths than the current CNAO treatment plan system. At CNAO, in order to reduce the extra dose delivered to the patient, a device is used (the chopper), that deflects the beam out of the extraction line, when the transition between consecutive spots is greater than $2\,\mathrm{cm}$. To take advantage of this device, a clustering method was implemented with the HyGA, which assumed that the chopper was used during the transition between clusters. This method was able to reduce by 2% the number of particles delivered with the CNAO treatment plan system. One of the drawbacks of using the chopper is the high percentage of particles. The SA and HyGA were able to reduce the particles wasted significantly. However, they presented an increase of 3% and 5% in the particles delivered with the CNAO treatment plan system.

Keywords : scan path optimization, algorithms, slice, irradiation spots.

Contents

List of Figures

List of Tables

Acronyms

SP	Selective Pressure.
CART-Lab	Computed Aided Radiotherapy Laboratory.
CERN	Organisation Européenne pour la Recherche Nucléaire.
CNAO	Centro Nazionale di Adroterapia Oncologica.
CX	Cycle Crossover.
DNA	Deoxyribonucleic Acid.
FSA	Fast simulated annealing.
FWHM	Full-Width-Half-Maximum.
GA	Genetic Algorithm.
GSI	Gesellschaft für Schwerionenforschung.
GSTM	Greedy Sub-tour Mutation.
GSX	Greedy Subtour Crossover.
HIT	Heidelberg Ion Therapy Center.
HyGA	Hybrid Genetic Algorithm with Heuristics.
IMPT	Intensity-Modulated Proton Therapy.
LET	Linear Energy Transfer.
MC	Monte Carlo.
NN-algorithm	Nearest Neighbor algorithm.
OER	Oxygen Enhancement Ratio.
OX	Order Crossover.
PB	Pencil Beam.
PIMMS	Proton Ion Medical Machine Study.
PMX	Partially Mapped Crossover.
RBE	Relative Biological Effectiveness.

SA	Simulated Annealing.
SOBP	Spread-Out Bragg Peak.
TP	Treatment Plan.
TPS	Treatment Plan System.
TSP	Travelling Salesman Problem.

Thesis Overview

According to the World Health Organization, cancer is a leading cause of death worldwide, accounting for 7.6 million deaths in 2008 [Org12]. It has been estimated that about 45% of all cancer patients can be cured (excluding those suffering from non-melanoma skin cancers). The standard methods for cancer treatment are surgery, chemotherapy and radiotherapy. Radiotherapy plays an important role since approximately 23% of all cancer patients are cured with radiotherapy (12% if used alone and 11% when combine with surgery or chemotherapy). Currently, the dominant radiotherapy, known as "conventional", uses photon beams[RBE08]. However, in the recent years, the interest in using accelerated charged particles [1], such as protons and carbon ions, has shown a considerable increase [PK11]. This interest can be attributed mainly to the characteristic depth-dose curve of these particles. It shows a low and nearly flat energy deposition in the entrance point and it increases with the penetration depth until it reaches a maximum (*Bragg peak*), and then it falls steeply to approximately zero[HKM11]. Confronted with this depth dose distribution and with the principle that the ideal radiation to treat cancer is the one that delivers a defined dose distribution within the target volume and none outside it, Wilson [Wil46] proposed the use of protons for high precision cancer therapy[Goi08].

Charged particle therapy has shown a remarkable growth: nowadays there are about 38 charged particle centres in the world, and more under construction [Gro12]. The Centro Nazionale di Adroterapia Oncologica (CNAO) is one of the first centres totally dedicated to charged particle therapy. In this centre, it is used the *active scanning technique* to irradiate the tumors. As it will be further explained in section 1.1.3, in this technique the target volume is divided into isoenergy slices containing a set of irradiation spots. The irradiation beam is then steered through each spot to cover the target volume slice by slice. An optimization of the path made by the irradiation beam (i.e. the scan path) can affect the treatment time, energy consumption and the extra dose delivered to the patient. This extra dose, depending on the type of *active scanning* technique, can be related with the irradiation of the slice during the transition between spots or with the time lag between the time when the prescribed particles are delivered and the time when the beam is turned off in each spot [IFT$^+$07]. A reduction in the scan path can be useful to decrease this extra dose delivered to the patient as well as the treatment time and energy consumption by the equipment. Therefore, in this thesis it is presented different optimization algorithms and the their impact on the scan path of real treatment plans from CNAO patients.

The scan path optimization was recently considered by two different studies [KWO07, PDB$^+$09]. The first study was done by Kang *et al.* [KWO07], where it was developed a method for minimization of the scan path by applying a Fast simulated annealing (FSA) optimization algorithm. This method was compared with the *zigzag algorithm* where the spots in each slice are irradiated line by line in consecutive rows. The developed method showed path lengths about 13%-56%

[1] In this work, by charged particles one should consider particles that have equal or higher mass than protons.

shorter than those of a zigzag pattern, leading to an improvement of the order of seconds in the treatment delivery time. The FSA algorithm also provided better solutions when the target geometry was irregular (irregular spot distributions in a slice), avoiding irradiation of unnecessary areas (areas without prescribed dose).

The second study was done by Pardo *et al.* [PDB+09] and it is similar to the previous one [KWO07]. However, it was used the classical Simulated Annealing (SA) instead of the FSA algorithm. The main difference between both algorithms relies in the definition of the survival probability. In SA a Boltzmann distribution is used while FSA rely on a Cauchy distribution.

Pardo *et al.* [PDB+09] study was focused on the best choice of operational parameters which the SA performance depends on. The convergence properties of the algorithm were further improved by using the next-neighbour algorithm to generate the starting paths. At the end, it was study the delivery dose distribution and the treatment delivery time using an optimized path. The performance of the method was also compared with the *zigzag* algorithm, showing that the implemented algorithm was able to optimize efficiently the scan path, leading to a better dose distribution and reduction of the treatment time.

The work here presented was developed at the Computed Aided Radiotherapy Laboratory (CART-Lab) group, whose main research is related to patient positioning and tumor tracking. This is a research group inside the TBMLab (Laboratorio diTecnologie Biomediche), which belongs to Politecnico di Milano. CART-Lab has different collaborations with hospitals and foundations, being the collaboration with the foundation CNAO the most important for this work [lab11]. At the moment, in CNAO only proton therapy is being performed and therefore, only information about patients treated with proton therapy was used.

Objectives

The main goal of the present work was to study the performance and the clinical implication of different optimization algorithms in real treatment plans from CNAO patients.

The secondary goals were:

- Comprehension of the main issues in path optimizations. Analysis of the current literature in order to identify possible optimization strategies for the problem.
- Implementation of the identified solutions.
- Evaluation of the performance of the implemented algorithms, using real treatment plans from CNAO patients.
- Study of the clinical implications of using the optimized paths.

- Development and implementation of a tool able to perform the scan path optimization using the competitive algorithms previously identified.

Outline

This thesis was divided into 5 chapters. In each chapter it is presented information that was consider relevant for the understanding of the scan path optimization problem and for the achievement of the proposed goals.

In order to introduce the scan path optimization problem into its context, chapter 1 summarizes some concepts behind charged particle therapy and optimization algorithms. In chapter 2, it is explained how the addressed problem is approached and which methods and materials are used to solve it. The results from the developed work are in chapter 3, whereas in chapter 4 the discussion of the results is given. Finally, chapter 5 reports the main conclusions to the work and future works.

1

Background Information

1.1 Charged Particle Therapy

This chapter offers a brief explanation of why charged particles are used in therapy and which techniques are used to make this possible.

1.1.1 Brief history

In 1946 Dr. Robert R. Wilson, a physicist who had worked on developing particle accelerators, suggested the use of protons and heavy ions as a possibility for radiation treatment. His argument was based on the depth-dose distribution presented by these particles (Fig.1.1) which could be suitable to treat tumors in humans [Wil46]. However, as shown in Fig.1.1, the *Bragg peak* is very narrow and usually not enough to cover most treatment volumes. Therefore, Wilson also proposed a technique, still used today, for modulation of the beam in depth. He proposed the use of a range wheel that creates beams with different energies and peak positions. When superimposed, the beams produce the Spread-Out Bragg Peak (SOBP) which provides an uniform dose to the tumor volume (Fig.1.2).

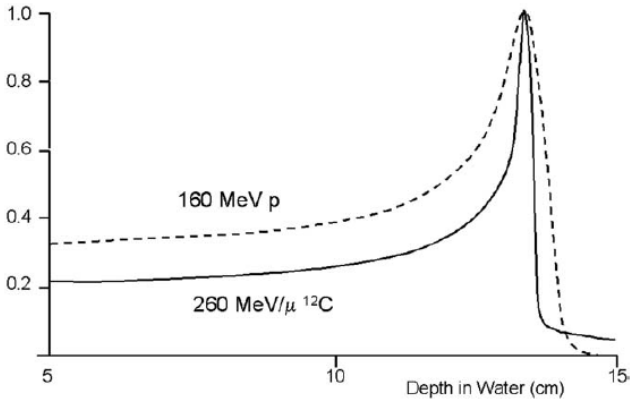

Figure 1.1: Relative depth-dose of monoenergetic charged particle beams. For protons, dashed line, and ^{12}C-ions, the full line. Adapted from [PK11].

It took less then 10 years for protons to be used to treat cancer patients for the first time [TLB+58]. However, despite the advantages of heavier ions the theoretical point of view, they were not well-understood clinically, therefore only in 1974, Joseph R. Castro and associates started to study therapy with heavier ions aiming to understand its clinical use. Between 1977 and 1992, several clinical experiences using heavy-ions (especially helium, carbon and neon ions) took place at the Lawrence Berkeley Laboratory, where encouraging results (mainly for skull base tumors and paraspinal tumors) were achieved [SEJS06]. However, the cost of developing and delivering heavy ions eventually could not be justified by the relatively limited number of patients leading to a slow development of charged particle therapy [Lin12].

Nowadays, due to the development of technology (e.g. accelerators and delivering technology), charged particle therapy with protons and carbon ions has gained again an increasing interest [KFM+10]. Worldwide there are about 38 therapy units that treat patients with charged particles (protons and carbon ions) and more than 75000 patients have been treated so far [Gro12].

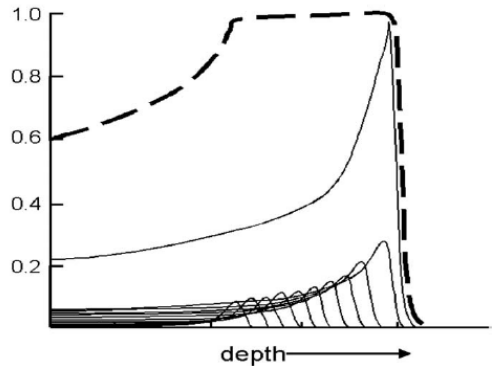

Figure 1.2: Spread-Out Bragg peak (dashed line) composed by composed a number of *Bragg peaks* with different energies. Adapted from [SEJS06].

1.1.2 Rationale of charged particles

The rationale of using charged particles in radiotherapy is related to the physical process of particle interaction (the physical rationale) and to the reactions (and its consequences) that occur at a cellular level after an irradiation with a charged particle beam (radiobiological rationale).

1.1.2.1 Physical Rationale

While charged particles travel through matter, they transfer energy to the medium due to atomic and nuclear interactions. This energy transfer is approximately inversely proportional to the square of their velocity [Tur07]. As they start slowing down, the probability of interaction increases. As a result of the accumulation of interactions, the particles stop and transfer the rest of their energy to the medium. This typical energy loss leads to a depth-dose curve with a sharp increase of dose at a well-defined depth (*Bragg Peak*) and a rapid dose falloff beyond that maximum (Fig.1.1). By positioning the *Bragg Peak* in the tumor it is possible to deliver a therapeutic

dose while sparing the surrounding tissues (Fig.1.3).

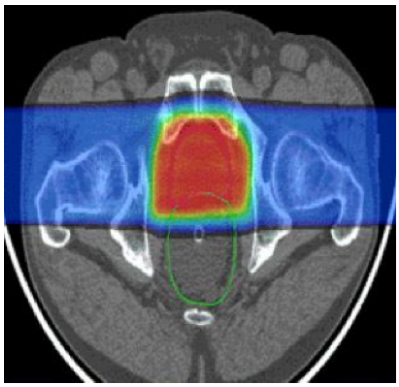

Figure 1.3: Treatment plan of a prostate tumor with proton therapy, using proton beams from 2 fields. The red area depicts the highest dose (around the prostate), followed by yellow, green and blue being the lowest dose. Adapted from [Onc12].

The depth and magnitude of the Bragg peak in a determined medium is the Bethe-Bloch equation (equation 1.1), which gives the mean rate of energy loss (or stopping power)[Tur07]

$$-\frac{dE}{dx} = \frac{4\pi k_0^2 Z^2 e^4 n}{mc^2\beta^2}\left[\frac{2mc^2\beta^2}{I(1-\beta^2)} - \beta^2\right] \tag{1.1}$$

The variables definition is in table 1.1.

Table 1.1: Quantities relevant for the Bethe-Bloch equation according to [Tur07]

Symbol	Definition
k_0	$8.99 \times 10^9\ Nm^2C^{-2}$
Z	atomic number of the medium
e	magnitude of the electron charge
n	number of electrons per unit volume in the medium
m	electron rest mass
c	speed of light in vacuum
β	speed of the particle relative to c
I	mean excitation energy of the medium

1.1.2.2 Radiobiological Rationale

When interacting with matter, radiation can damage tissues by direct or indirect action (Fig.1.4). In direct action, the Deoxyribonucleic Acid (DNA) molecules are directly ionized, being therefore damaged by the ionizing particles[Cre05]. Since DNA is found in almost all the cell and is responsible for the function that each cell performs, the damaged made in the DNA either kills the cell or turns it into a different kind [sit12]. In indirect action, the radiation interacts with other molecules and atoms, mainly water, within the cell producing free radicals that can damage the DNA cells. However, to make the DNA damage permanent, further reaction with oxygen is required to prevent the DNA to repair itself [OzR12].

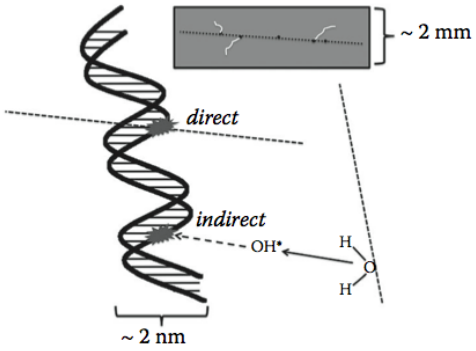

Figure 1.4: Direct and indirect (via diffusion of free radicals) radiation effects on DNA. Adapted from [Pag12].

The effect of radiation in oxygenated and hypoxic tumors[1] can be modeled through the Oxygen Enhancement Ratio (OER) concept. The OER of radiation is given by the ratio between the dose D required to produce a certain biological effect E in the absence of oxygen and the dose required to produce the same effect in the presence of oxygen[Lin12],

$$OER = \frac{D_{hypoxic}}{D_{oxygen}} \tag{1.2}$$

As one can see in Fig.1.5 for Carbon ions, in opposition to X-rays, the survival curves for air (oxygenated environment) and nitrogen atmosphere (hypoxic environment) do not differ much (low OER). The reason behind this fact is because Carbon ions are considered to be high-LET particles.

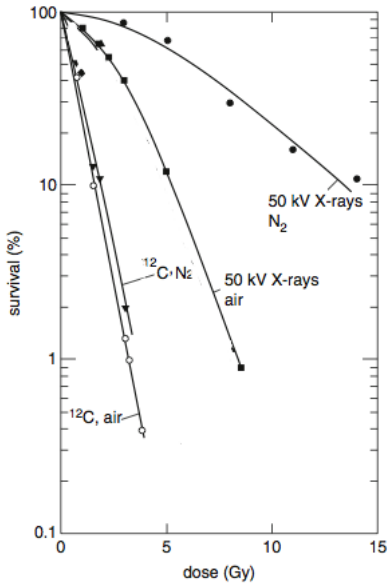

Figure 1.5: Cell survival curves of human kidney T1 cells after irradiation with ions or X-rays in air or nitrogen atmosphere, respectively. Adapted from [Lin12].

[1] As a tumor grows, it rapidly outgrows its blood supply, leaving normally in large tumors a central cores that lack in oxygen [Cre05].

The Linear Energy Transfer (LET) is a measure of the energy that is transferred by an ionizing particle to the medium where it travels [Lin12]. For high-LET radiation, the DNA damage is mainly caused by direct action. Whilst for low-LET radiation (like X-rays and protons) about two-thirds of the damage is caused by indirect action. It is due to this factor that high-LET radiation presents smaller OER. This reduction in OER and the fact that high-LET particles produce greater damage to cells than low-LET particles, have become one of the main reasons behind to use high-LET radiation in cancer therapy [Lin12].

Another important measure used to qualify the radiation damage and its effect in tissues is the Relative Biological Effectiveness (RBE).

As it is possible to see in Fig.1.5, the fraction of cells surviving a particular dose of photon (D_{photon}) is larger than the fraction of cells surviving the same dose of charged particles ($D_{particle}$) [HKM11]. This means that charged particles are biologically more effective than photons, being necessary a lower dose to achieve the same biological effect [SEJS06]. Therefore, a parameter which compares the biological effectiveness of charged particles to photons called RBE was defined. The RBE can be written as [HKM11]:

$$RBE = \frac{D_{photon}}{D_{particle}} \tag{1.3}$$

The RBE depends on the type of particle (underlying LET), cell type and delivered dose. For proton therapy, the generic RBE of protons is 1.1, however due to the dependency on the aforementioned parameters, this value can vary by about 10% to 20% [PG00]. The dependence on the various physical and biological properties of RBE for heavy ions (such as carbon) is much stronger than for protons. They show diverse RBEs as they travel through matter. Under specific conditions the RBE can be approximated to be only a function of depth (for more information: article [SEJS06]).

1.1.3 Treatment delivery systems

After the extraction of the beam from a particle accelerator, this is guided to the treatment room and to the patient using magnets which bend, steer and focus the particle beam. The success of cancer treatment in radiation therapy is strongly related to the possibility of applying the beam to the target volume using multiple fields [SEJS06]. The use of a gantry which rotates around the patient offers this possibility. However, gantries for charged particles are of great size and weight. A proton gantry weights around 100 tons and has a diameter of 10 meters, whereas an isocentric gantry for carbon ions has a weight of about 600 tons and a diameter of 13 meters [Rob12]. The enormous size and weight of a gantry for heavy particles, is one of the reasons why till 2010 only one heavy-ion center (Heidelberg Ion Therapy Center (HIT)) had a gantry for cancer treatment [KFM$^+$10] (figure 1.6). Therefore, in heavy-ion centers fixed beam lines are typically used: vertical beams, 45° beam inclination and horizontal beams. Moreover, it is

possible to move the patient using special treatment chairs [GSI11].

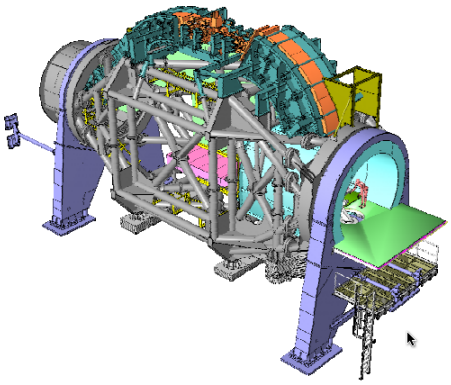

Figure 1.6: Drawing of the heavy ion gantry at HIT including mechanics, beam line components and patient treatment room. Adapted from [WK08]

The beam produced in the accelerator has a small diameter and small extension of the Bragg Peak in depth, being necessary to shape the beam in order to be useful for treatment.

Nowadays, in charged particle therapy, there are two methods to shape the beam and thus to tailor the dose to the target volume: *passive scattering* and *active scanning* techniques [KWO07].

1.1.3.1 Passive Scattering

Passive scattering (Fig.1.8) was the first method to be developed and is still broadly used in charged particle therapy centers. In this technique a ridge filter and/or range shifters are used, which are responsible to modulate the beam to the desired radiological depth (or SOBP). These range modulators consist of a number of homogeneous plastic plates of different thickness, that can be moved into the beam (Fig.1.7).

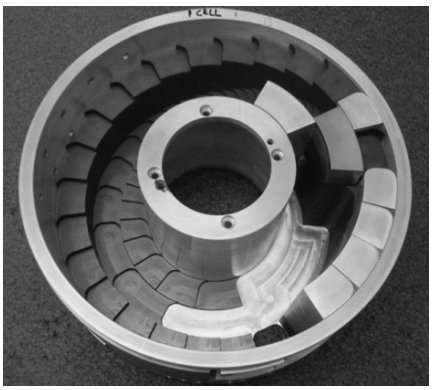

Figure 1.7: Range modulator wheel combining three range modulation tracks. Adapted from [Pag12].

.

The lateral spread out of the beam to cover homogeneously the whole target can be produced by interposing scattering material in front of the beam (*single scattering* and *double scattering* techniques see [Goi08] for more information). Furthermore, patient and beam-specific collimators are used to adapt the dose distribution the maximal lateral cross section of the target volume.

Variations in depth of the distal edge of the target volume are mapped to the dose distribution by a patient and beam-specific device, the compensator. The distal edge of the dose distribution can be adapted very precisely to the prescribed target volume, but due to the fixed width of the SOBP, this shape is transferred to the proximal edge of the dose distribution, resulting in an unwanted irradiation of proximal normal tissue (Fig.1.8, dark red) [Gro05].

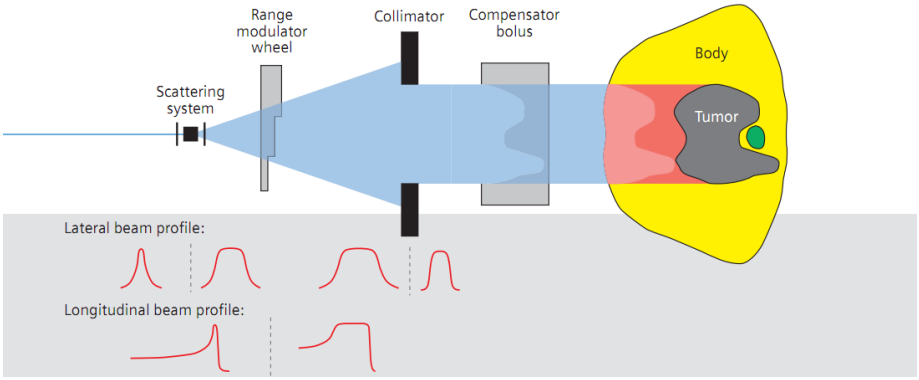

Figure 1.8: Principle of passive scattering (upper part: schematic setup; lower part: variation of lateral and longitudinal beam profile along. Adapted from setup [Gro05].

Instead of using a scattering system for the lateral spread of the beam, it is possible to use fast, continuous magnetic deflection (wobbling), that move the beam over a defined area (Fig.1.9) [SEJS06].

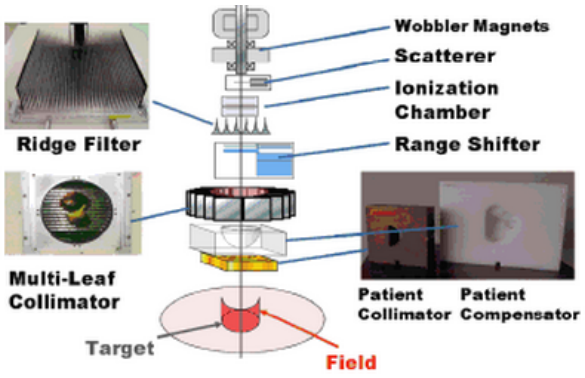

Figure 1.9: Principle of passive shaping with wobbling system. Adapted from [CC09].

.

Whilst passive scattering has proved to be robust, there are some important disadvantages: the cumbersome use of patient-specific collimators and compensators, the significant beam energy and intensity losses, the contamination in the beam by fragments, and neutron production in the scattering material, leading to an unnecessary neutron dose [KWO07].

1.1.3.2 Active Scanning

In *active scanning* (Fig.1.10) there are two dipole magnets connected in series which steer the narrow pencil beams in the lateral plane while the range is modulated by controlling the beam energy [Goi08]. This minimizes the equipment required and automates the treatment

delivery process by a control system [KWO07]. The target volume is virtually divided into slices of constant particle range (and energy), the so-called isoenergy slices. Each of these slices is further divided into single picture elements (pixels or spots). The beam is then steered over each slice in a way that a precalculated number of particles is deposited to every spot assigned by the treatment plan [Gro05].

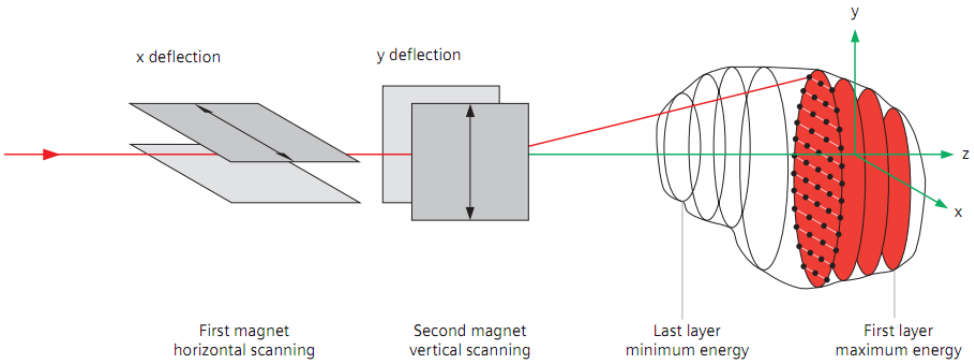

Figure 1.10: Principle of active beam scanning. Adapted form [Gro05].

Active scanning can be divided into two categories: *Discrete* or *spot scan*, where the beam is turned off during the scanning between consecutive spots, and *raster* or *quasidiscrete scan* where instead of turning off the beam between consecutive spots, this is only turned off when a slice is finished and a new energy is set [KWO07].

In *Active Scanning* the dose distribution is delivered by placing the Bragg peak in the patient one location at a time and then one layer at a time by varying the beam energy, thus allowing the use of Intensity-Modulated Proton Therapy (IMPT). With IMPT the uniform dose distribution over the target volume is constructed only by the combination of two or more treatment fields (different irradiation angles). Each individual field can deliver a highly inhomogeneous dose distribution to the target, but when combined lead to a uniform dose over the target [Pag12].

1.1.4 The CNAO facility

The Centro Nazionale di Adroterapia Oncologica (National Centre for Oncological Hadrontherapy), better known as CNAO, is a synchrotron-based oncological treatment center which uses charged particles with the *quasidiscrete scanning* delivery technique [GAA+08]. It is the first hospital in Italy (and sixth in the world after United States of America, Germany and Japan) specifically dedicated to cancer treatment using heavy-ions [Wik11a].

The idea of an Italian hadrontherapy center dates back to 1991 when professor Ugo Amaldi made the first proposal [AT91]. In 1992 the TERA foundation [TER11] (TErapia con Radiazioni Andoniche, which in English means Therapy with hadronic particles) was created, a non-profit foundation whose main purpose is the introduction of the most recent techniques to treat cancer in Italy and Europe. Later in 1994, the TERA foundation was recognised by the Italian Ministry

of Health [Pul08].

In 1996, Organisation Européenne pour la Recherche Nucléaire (CERN) [CER11], med-austron and TERA started the Proton Ion Medical Machine Study (PIMMS) in collaboration with Gesellschaft für Schwerionenforschung (GSI) and Onkologie-2000 which joined later the study group. This study lasted approximately four years and its aim was to design an accelerator (synchotron) and the beam lines of a proton and carbon ion hadron therapy center, without any financial and/or space limitation [Ama01].

In 1997, on the basis of the ongoing work of PIMMS, the TERA foundation proposed the construction of the CNAO in Italy, based on the PIMMS system, but less expensive. In 2001, with the financial law, the Italian Ministry of Health created a non-profit organization, named CNAO foundation, to build and subsequently run the National center for Hadrontherapy [Pul08].

The CNAO is located in Pavia and its inauguration took place in 15^{th} of February, 2010. However, the first patient was only treated in September 2011 with protons [Pic11]. Other patients have been treated so far and the CNAO has commenced enrolling patients into clinical protocols approved by the Ministry of Health for the use of proton beams. Currently, CNAO plans to activate new clinical protocols and implement a new phase of treatment using carbon ions[2]. By the end of 2012 it is envsion that the clinical trial phase is over, leading to the next phase of the Centre's operation that will treat about 3000 patients per year, expand the clinical indications and conduct clinical radiobiological and technology research activities [CNA12].

The CNAO has three treatment rooms equipped with horizontal fixed beam outlets; one of them houses an additional beam line from above (vertical). Siemens Healthcare supplied the treatment planning program, the *syngo PT Planning* for scanned protons and carbon ions in 2009 [Hea11].

A collaboration with the CNAO center allows access to patient treatment plans which can be used for testing the optimization algorithms.

1.1.5 Dose Calculation: Pencil Beam Algorithm

As already stated, at CNAO it is used an *active scanning* technique to irradiate the target volume. In active scanning many (up to tens of thousands) narrow particle beams are used for irradiation [Ǵ11]. A simple method that has been broadly used in proton therapy for dose calculation is the Pencil Beam (PB) algorithm.

Different PB algorithms have been considered [HGB$^+$96, SFA05] in radiotherapy, however they all rely on the same principle. In a PB algorithm the total dose delivered to an irradiated area is the sum of the dose given to each irradiated spot plus the dose contribution of each pencil beam used for irradiating the adjacent spots. A *pencil beam* irradiating a spot p_1 can contribute

[2]Currently, only proton therapy is being done

to the dose of an adjacent spot p_2. The reason behind this is mainly because charged particles while traversing a medium suffer elastic scattering due to the interactions with the electric field of atoms [Att91]. This scattering leads to a spatial distribution of the pencil beam that can be approximated to a Gaussian distribution (Fig.1.11)[Pag12].

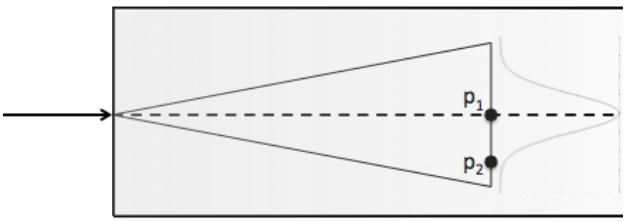

Figure 1.11: Representation of the lateral distribution of charged particles when traversing a medium. For small-angle scatter, the distribution is approximately Gaussian.

Therefore, the dose of each pencil beam to a point/spot p, can be stated as follows [Pag12]:

$$D(p) = \frac{W}{2\pi\sigma^2} exp\left(-\frac{r_p^2}{2\sigma^2}\right) D_\infty(p) \tag{1.4}$$

where W is the dosimetric weight of the pencil beam (physically proportional to the number of protons in the pencil beam), $D_\infty(p)$ is the depth dose contribution in p (given by the depth-dose curve, Fig.1.1), r_p is the distance from the pencil beam axis to p and σ is the spread of the pencil beam at depth p.

The depth-dose distribution D_∞ can be obtained by experimental data [HGB$^+$96] or by precalculated [SA07] curves generated by Monte Carlo (MC) methods.

MC algorithms are the most accurate methods of simulating particle interactions within a medium. In a MC method, individual particles are tracked (one by one, step by step) as they penetrate through the patient and interact with the material through which they pass. The likelihood of an interaction (selection of which interaction the particle must suffer), and its consequences, is randomly sampled from one or more probability distributions [Ǵ11, Pag12].

The complete dosimetric study could be developed by a MC method, which had already proved to be more accurate than a PB algorithm [PJP$^+$08]. However, the implementation of a MC algorithm can not be trivial and in order to obtain sufficient statistical accuracy for useful dose distributions (depth and lateral) in practical situations, tens of millions of particles usually must be traced. Such calculations can take hours or even days to process [Ǵ11, PJP$^+$08].

1.2 Optimization Algorithms

1.2.1 The Travelling Salesman Problem

The scan path optimization problem can be viewed as a Travelling Salesman Problem (TSP). The travelling salesman problem is combinatorial optimization that was first formulated as a mathematical problem in 1930 and is one of the most intensively studied problems in optimization [Wik12b]. The classical formulation of the TSP can be denoted as follows:

Given a set of N *cities and the travel cost (or distance) between each possible pair of cities, the task of the TSP is to find the best possible way of visiting all the cities exactly once and returning to the origin city while trying to minimize the travel cost (or travel distance).*

The total number of possible routes covering all cities is given by $(N-1)!/2$, which makes the search for the exact solution impractical [Dav10]. Therefore, different optimization algorithms have been proposed in order to solve it satisfactorily.

As it will be later explained in section 2.1, in the scan path optimization the irradiation spots in each slice can be treated as the cities that must be visited by the irradiation beam. However, in this case it is not necessary to return to the initial spot. To solve this optimization problem it was considered different optimization algorithms that will be explained below.

1.2.2 Simulated annealing

The SA is an heuristic algorithm, which guarantees the convergence to a near-optimal solution in a reasonable time. The SA algorithm also has the ability to avoid trapping in local minima. The name and principle of SA come from annealing in metallurgy. It is a technique involving heating and controlled cooling of a material to increase the size of its crystals and reduce their defects. [Wik11c]. At high temperatures, the atoms become unstuck from their initial positions (a *local minimum* of the internal energy) and move freely with respect to one another through states of higher energy. With a decrease in the temperature, the thermal mobility is lost, therefore it is important to assure a slow cooling, which gives to the atoms more changes of finding configurations with lower internal energy than the initial one, forming a crystal. This crystal is the state of minimum energy for this system [PTVF07].

In an optimization problem, the objective function, is the equivalent of the internal energy, which needs to be minimized. A control parameter T needs to be defined and it will play the role of the temperature. The algorithm starts from a possible solution (possible path), where at a fixed temperature, random perturbations lead to a new path (rearrangement of the atoms, in the annealing process). If this new path corresponds to a lower value of the objective function it is accepted, while if it results in a higher value, this new path is accepted with a probability depending on the control parameter, T (usually, the probability is according a Boltzmann distribution).

After a pre-defined number of cycles, or if the number of accepted paths/solutions (number of successes) reaches a pre-defined value, the control parameter, T, is decreased and the later process is repeated, where the initial solution is now set to the path configuration obtained before [PTVF07, PDB+09].

1.2.3 Genetic Algorithms

Genetic Algorithm (GA) was first introduced by John Holland for the formal investigation of mechanisms of natural adaptation [Hol75]. Nowadays, GAs are routinely used to generate useful solutions to optimization and search problems [Wik11b]. GAs are based on the principle of "Survival of the fittest", introduced by Charles Darwin [Dar59]. According to this principle, in nature the *fitness* is related to the ability of an individual to survive and reproduce. Nevertheless, there is a small probability of survival of the less *fitted*. The GAs can be described as a process with the following steps:

- Encoding;
- Selection;
- Crossover;
- Mutation;

1.2.3.1 Encoding

The first step when using a genetic algorithm is to create the initial population which contains the individuals that will lead to the future generations. Each individual is a possible solution for the optimization problem. The encoding is related to the way each individual is represented. This process is one of the most difficult aspect of solving a problem using genetic algorithms. In the crossover process, a non appropriate representation of the individuals/solutions will lead to impossible configurations. There are different ways to represent each individual/solution in the population, however for the present work it will be only considering the path representation [Bry00] (section 2.1.1 in chapter 2).

1.2.3.2 Selection

Selection consists in selecting the individuals of the present generation (or population) that will participate in the next operations: *crossover* and *mutation* [ADA08]. The selection is done taking into account the *fitness* value, which is given by the optimization function.

1.2.3.3 Crossover

After two individuals being selected from the population (hereafter, called the parents), they may or may not, exchange exchange partial structures randomly selected to produce two new individ-

uals/offspring [ADA08]. This exchange is called crossover process and can happen according to a certain probability - *crossover probability*.

1.2.3.4 Mutation

Mutation occurs after crossover and as in nature it exchanges alleles/spots randomly [ADA08]. It is used in order to avoid the optimization process being trapped in a local optimum. Due to the randomness of the process, it is normal that occasionally some paths will be near a local optimum but and none near the global optimum. Therefore, it is introduced the possibility of mutation for the possible solutions. The mutation is random process that occurs according to a certain probability -*mutation probability*. It allows a larger diversity in the solutions avoiding the local optimum trap [Bry00].

1.2.4 Nearest neighbour and 2-opt algorithms

The Nearest Neighbor algorithm (NN-algorithm) is one of the oldest and most intuitive optimization algorithm that was first introduced by Rosenkrantz *et al.* [Goe11]. In the context of the TSP problem the NN-algorithm can be described as follows:

Given a starting city, according to this algorithm the next city to be visited is the one that has a smaller travel cost (or the closest one). This procedure is repeated till all the cities were visited.

The NN-algorithm is a greedy algorithm. A greedy algorithm tries to solve a problem by making the locally optimal choice at each stage with the hope of finding a global optimum. However, a sequence of optimal single-step actions may not lead to a global optimal solution. For instance, different starting points may lead to different solutions and none be the optimal solution [Goe11].

The 2-opt algorithm was first proposed by Croes [Wik12a] to solve the travelling salesman problem. It is a local search algorithm, which tries to improve a route by applying local changes, until a solution deemed optimal is found. In piratical terms, the main idea of this method is to take a route with intersections (route that crosses over itself) and reorder it so that it does not have intersections (Fig.1.12).

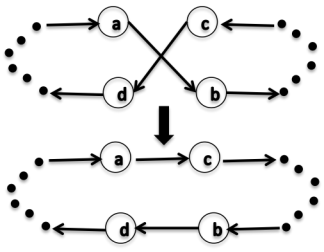

Figure 1.12: The 2opt method.

2

Methods and Materials

In this chapter the methods and materials used in this study will be described. All the data used was obtained from real treatment plans of CNAO's patients.

2.1 Scan path optimization

The optimization of the scan path of a 3D target volume can be approached as a variation of the travelling salesman problem (see chapter 1.2.1 in page 11). A complete 3D scanning sequence is just the sum of all 2D scanning maps (energy slices) over all beam angles. Thus, the 3D scan path optimization problem can be naturally subdivided in a sequence of independent 2D TSPs, which is much faster to solve and simple. The scan path for each slice is optimized independently from the other slices. In this way, the 3D path optimization is reduced to two dimensions. Considering one slice with N irradiation spots, the position of each irradiation spot is given by the Cartesian coordinates (x_i, y_i), with $i = 1, 2....N$ (e.g. Fig.2.1). The distance between each two spots is given by:

$$d = \sqrt{(x_i - x_{i+1})^2 + (y_i - y_{i+1})^2} \tag{2.1}$$

Therefore, the total path length (f) is given by:

$$f = \sum_{i=1}^{N-1} \sqrt{(x_i - x_{i+1})^2 + (y_i - y_{i+1})^2} \tag{2.2}$$

This equation is the objective function to be minimized.

2.1.1 Encoding

The encoding process is related to the way possible solutions are represented. For the applied methods it was used the path representation, where the irradiation spots are numbered $i = 1, 2, ...N$, being N the number of spots per slice [LKM$^+$99]. Therefore, a possible scan path is a

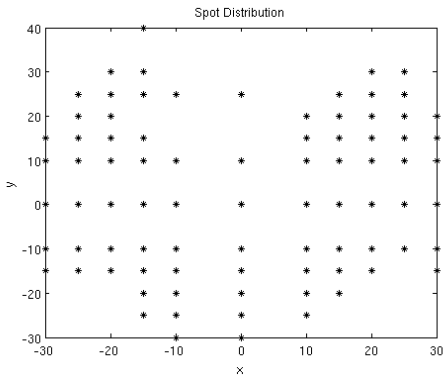

Figure 2.1: Scheme of a spot distribution.

permutation (with no repetition) of N values. Each value corresponds to a irradiation spot, which in turn is represented by the Cartesian coordinates (x_i, y_i).

2.1.2 Simulated Annealing

The implementation of this algorithm, as well as the selection of the operational parameters, were based in the study developed by Pardo [PDB+09]. The implemented pseudo-code is in Fig.2.2

For a given slice with N irradiation spots,

1. Generate a starting path P_0;
2. Start the decreasing temperature loop, with a $T = T_0$;
   (a) Start the random perturbation loop;
      i. Obtain a new path P by performing a random arrangement in P_0;
      ii. Compute $\Delta = f(P) - f(P_0)$ (equation 2.2);
      iii. If $\Delta \leq 0$, set $P_0 = P$ and the number of success is increased by one;
      iv. Else, choose a random number $r \in [0, 1]$. If $r < e^{-\Delta/T}$, set $P_0 = P$ and the number of success is increased by one;
   (b) End of the random perturbation loop, if the number of iterations is over or if the number of allowed success is reached.
   (c) Decrease the temperature according to equation 2.3;
3. End of the decreasing temperature loop if the number of iterations is reached.

Figure 2.2: SA pseudo-code.

The decrease in temperature in each iteration (i) is given by:

$$T = a^i T_0; \tag{2.3}$$

where $a = 0.9$ and $T_0 = 0.5$ according to Pardo study[PDB$^+$09].

In the decreasing temperature loop it was considered 1000 iterations, while for the random perturbation loop, $100 \times N$ iterations and $10 \times N$ success were considered. As path rearrangement it was used two possible path configurations, each one with a 50% probability of being selected. The two path rearrangements were the following:

1. A path segment of size n is removed from the path and replaced with the same segment in reverse order.
2. A path of size n is removed and then replaced between two other spots, randomly chosen. n is a random integer from 4 to N;

According to recent studies [GGKL05, PDB$^+$09], the convergence of an optimization algorithm can be faster if the initial solutions are already "good" solution. Therefore, to create the starting path it was considered the NN-algorithm (section 1.2.4).

In the present work, the algorithm was implemented using C++ language.

2.1.3 Genetic Algorithms

It was implemented a standard GA to solve the scan path optimization. The implemented pseudo-code can is shown in Fig.2.3.

The *fitness* function is given by equation 2.2. Shorter the path length, higher is its *fitness* value. For the selection process it was considered a linear rank-based roulette method, which sorts the population according to their fitness rank. The fitness rank (equation 2.4) of each member in the population is calculated taking into account their fitness value (equation 2.2) and a controlling parameter - the Selective Pressure (SP). The SP values is responsible for controlling the biasness and can be a value between 1 and 2. The pseudo-code of the rank-based roulette is shown in Fig.2.4.

$$Fitness\_Rank(Pos) = 2 - SP + 2 \times (SP - 1) \times \frac{Pos - 1}{N - 1} \tag{2.4}$$

For a given slice with N irradiation spots,

1. Generate a starting population P_0, that contains N_{pop} possible paths;
2. Set the number of iterations (N_{it}) to zero.
   (a) Compute the *fitness* function of each individual in P_0 (equation 2.2);
   (b) Select two individuals from P_0 taking into account their *fitness* value.
   (c) If a random number is lower then the crossover probability P_c
      i. Crossover the two selected individuals, which will lead to two new offsprings;
      ii. If a random number (between 0 and 1) is lower then the mutation probability P_m, mutate both offsprings;
      iii. Replace in P_0, the two less fitted individuals by the two offsprings;
   (d) Repeat the process until N_{it} equals the stopping criteria.

Figure 2.3: GA pseudo-code.

For a population with N possible paths:

1. Order the paths in the population taking into account their *fitness* value (equation 2.2). To the least fitted assign the first position ($Pos = 1$), while to the fittest the last, $Pos = N$;
2. Calculate the ranking of each path (equation 2.4) and normalize the ranking values to its cumulative sum;
3. Sum the ranking values of each path, according to the previous established order, till the sum exceeds a random number between zero and one;
4. The path in which the summing process stopped is the one selected for crossover;
5. Repeat as many times necessary.

Figure 2.4: Rank-based roulette.

For crossover three different methods were tested: Partially Mapped Crossover (PMX), Order Crossover (OX) and Cycle Crossover (CX).

Order Crossover (OX) This method was proposed by Davis [Dav85]. The offspring is built by choosing a subsequence of a tour from one parent and preserving the relative order of the other parent. An example of how this crossover method works is shown in Fig.2.5a.

Cycle Crossover (CX) This method was first proposed by Oliver [OSH87], where the offsprings are build in such a way that each spot (and its position) comes from one of the parents. In Fig.2.5b it is shown an example of how this algorithm works. The algorithm starts from copping into the offspring 1 the first position of parent 1. Then it checks which spot is in the first position in parent 2 and search it in parent 1 and once again copy it into offspring 1. This process continues till the offspring is complete or a repetition is found (red dashed arrow). In the later case, the empty positions in the offspring 1 are filled with the spots in parent 2 that were not used. For the second offspring it is followed the same method but the starting spot is from parent 2.

Partially Mapped Crossover (PMX) This method was proposed by Goldberg and Lingle [GL85]. In this method an offspring is built by choosing a subsequence of a tour from one parent and preserving the order and position of as many spots as possible from the other parent. As in the OX method, two random cut points are used to define the subsequence that will be copied. The sub-tours in each parent are called *mapping sections*, because they will give a map that will be used to legalize the offspring (red arrows). An example of this method is in Fig.2.5c.

As in the SA methods, the initial population was created using a NN-algorithm. The GA algorithm was applied using Matlab®.

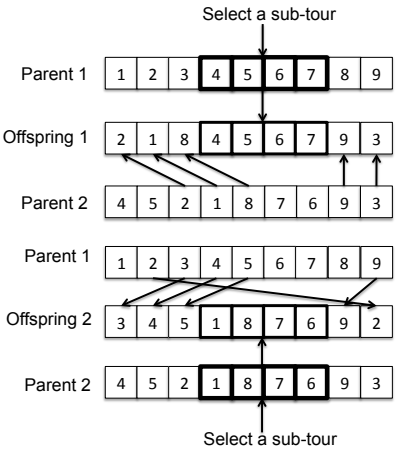

(a) Order Crossover method.

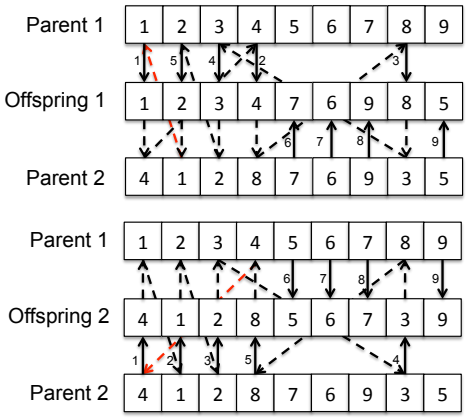

(b) Cycle Crossover method.

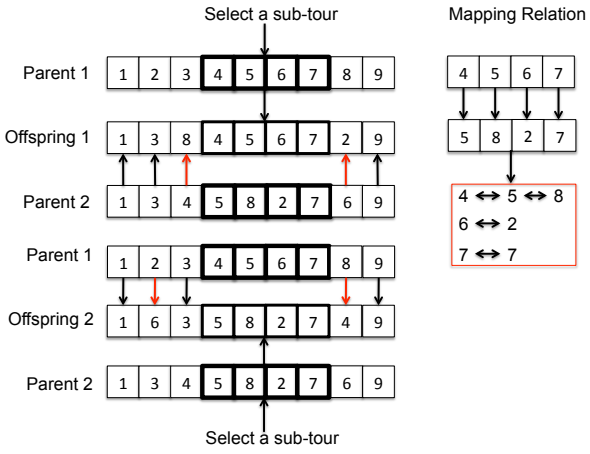

(c) Partially Crossover method.

Figure 2.5: Different Crossover methods. The sub-tours are randomly selected.

2.1.4 Hybrid Genetic Algorithm

The objective of using a hybrid algorithm is to combine the best characteristics of different algorithms. In order to speed up the convergence of the GA it was implemented two hybrid methods: The Genetic Algorithm with Greedy Sub-tour Mutation (GSTM) and the Hybrid Genetic Algorithm with Heuristics (HyGA).

2.1.4.1 Genetic Algorithm with Greedy Sub-tour Mutation

This hybrid algorithm uses the genetic algorithm described in Fig.2.3 with a greedy mutation method - GSTM. This method was proposed by Albayrak and Allahverdi [AA11], and tries to improve the path every time there is the mutation process. Its pseudo-code is described in Fig.2.6 to Fig.2.9 while in table 2.1 shows the definition of the used variables.

For each offspring:

1. Select randomly a sub-tour;
2. If $Rnd \leq P_{RC}$
   (a) Subtract the sub-tour from the offspring (Fig.2.7b);
   (b) Reconnect the sub-tour to the offspring in such a way that the total path length is minimal (Fig.2.7c);
3. Else
   (a) If $Rnd \leq P_{CP}$
      i. Perform the random distortion algorithm (Fig.2.9);
   (b) Else
      i. Select one neighbour (NL_{R1} and NL_{R2}) from each neighbour list (Fig.2.8a);
      ii. Invert the path (Fig.2.11b) making NL_{R1} and NL_{R2} being connected with $R1$ and $R2$ respectively (Fig.2.8b and 2.8c);

Figure 2.6: GSTM pseudo-code. Adapted from [AA11].

Table 2.1: Variables that are relevant for the GSTM algorithm [AA11].

Symbol	Definition	Value
Rnd	Random number	[0,1]
P_{RC}	Reconnection probability	0.5
P_{CP}	Correction and perturbation probability	0.8
P_L	Linear probability	0.2
R_1	First spot of the sub-tour	-
R_2	Last spot of the sub-tour	-
NL_{R1}	Spot from the neighbour list of R_1	-
NL_{R2}	Spot from the neighbour list of R_2	-

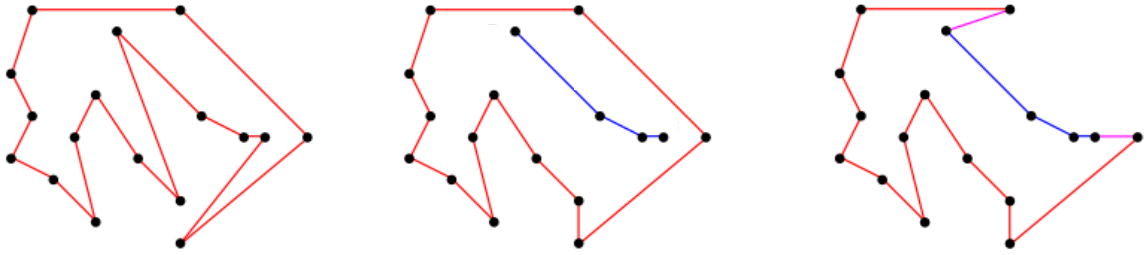

(a) Original Path.

(b) Removal of a random sub-tour.

(c) Reconnection with the path in a way the total path length is minimal.

Figure 2.7: Greedy reconnection. Adapted from [AA11].

Set $w = R_1$;

1. If $Rnd \leq P_L$
   (a) Select randomly a spot from the sub-tour and set the w position of the offspring to this value;
2. Else
   (a) Set w position of the offspring to the last spot of the sub-tour;
3. Remove the spots from the sub-tour that were already selected and set $w = w + 1$;
4. Repeat the process while there are spots in the sub-tour.

Figure 2.9: Random distortion algorithm.

The method was implemented in Matlab®.

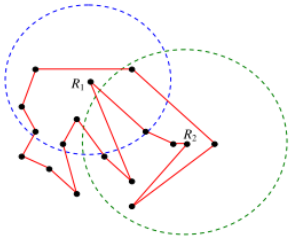

(a) Neighbour list of R_1 (dashed blue circumference) and R_2 (dashed red circumference). Neighbourhood's size = 7.

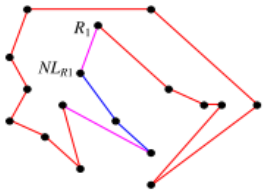

(b) Reconnection by the inversion method of NL_{R1} with R_1.

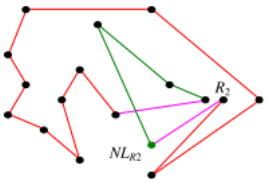

(c) Reconnection by the inversion method of NL_{R2} with R_2.

Figure 2.8: Sub-tour inversion and neighbour list. Adapted from [AA11].

2.1.4.2 Hybrid Genetic Algorithm with Heuristics

The HyGA was proposed by Sengoku and Yoshihara [SI93] and combines a genetic algorithm with a 2opt method. The pseudo-code of this algorithm is described in Fig.2.10. For crossover it was consider the Greedy Subtour Crossover (GSX) method which was also proposed by Sengoku and Yoshihara [SI93] (Fig.2.12).

The mutation was done by using the the 2opt method (section 1.2.4) that improves a path by detecting and undoing the intersections found (Fig.2.11). An intersection can be identified when $\overline{W_{i+r}W}_{i+r+1} + \overline{W_iW}_{i+1} > \overline{W_{i+r}W}_i + \overline{W_{i+r+1}W}_{i+1}$ is satisfied.

The algorithm was implemented in Matlab®.

For a given slice with N irradiation spots,

1. Generate a starting population P_0, that contains N_{pop} possible paths;
2. Elimination of $N_{pop} \times p_e\%$ paths from the population taking into account their *fitness* value (i.e. the path length given by equation 2.2). The new population P has $N_{pop} \times p_e\%$ less possible solutions than P_0.
   (a) The paths are sorted according to their path length;
   (b) The path length of adjoining paths is compared. If the difference is less than ε (a small positive real number), the preceding path is eliminated while the number of eliminated paths is less than $N_{pop} \times p_e\%$. If the total number of eliminated paths is lower than $N_{pop} \times p_e\%$, then the paths with the lowest path length are eliminated till the total number of eliminated paths reaches $N_{pop} \times p_e\%$.
3. $N_{pop} \times p_e\%$ solutions are selected from P for Crossover. The resultant $N_{pop} \times p_e\%$ offsprings are added to the population P, which will now have N_{pop} individuals.
4. $N_{pop} \times p_i\%$ solutions are selected from P for Mutation. The best solution (lower path length) is always selected from P.
5. Set P to P_0 and go to step 2. Repeat till the total number of iterations is reached.

Figure 2.10: HyGA pseudo-code. Adapted from [SI93].

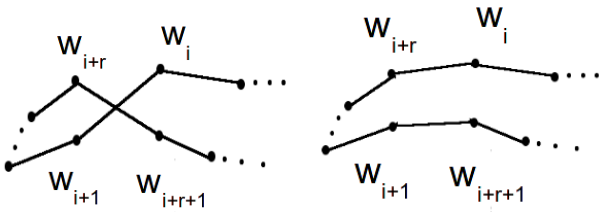

(a) Intersection. **(b)** Non-intersection.

Figure 2.11: Inversion method. W represents the spot and the subscript represents the path order: $1,2...,i,i+1...i+r-1,i+r,i+r+1....N$. Using the inversion method [CH06], the path is modified to $1,2...,i,i+r,i+r-1...i+1,i+r+1....N$.

1. Select a random spot, $t = 6$, and copy it into the offspring;
2. Identify the position where $t = 6$ is placed in each parent: x_1 and x_2. Set $x_1 = x_1 - 1$ and $x_2 = x_2 + 1$;
3. Place the spot in position x_1 on the left side of the spots already in the offspring. Do the same with x_2 but place it on the right side;
4. Repeat this process while the offspring's size is not the same of its parents or if one of the selected spots is already in the offspring.
5. If the offspring still does not have the same size as its parents, add randomly the rest of the "unpicked" spots.

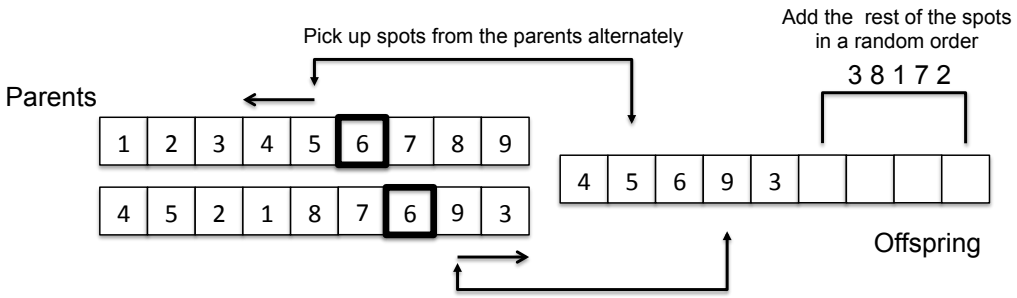

Figure 2.12: Greedy Sub-tour Crossover. Adapted from [SI93]

2.2 Clinical Cases

The data used to assess the performance of the optimization algorithms was obtained from treatment plans of real patients at CNAO. The Treatment Plan System (TPS) used in CNAO is the *syngo PT Planning*, manufacture by *Siemens AG, Healthcare Sector, Oncology Care Systems*. In each Treatment Plan (TP) it is possible to obtain information about the number of slices, the scanning path and spot distribution in each slice, the number of particles prescribed to each spot

and the beam Full-Width-Half-Maximum (FWHM), intensity and energy.

As already mentioned, in *quasidiscrete scanning*, the beam is not turned off during the irradiation of each slice. However, clinically at CNAO when the distance between two consecutive spots is greater than $2cm$, a device called *chopper* is used. The chopper deflects the beam out of the extraction line, avoiding irradiation of the tumor during this transition. The beam is still steered between the two consecutive spots (without delivering particles), contributing for the total path length.

The possibility of using the chopper during irradiation was taken into account in the particle distribution study. The use of chopper was consider in two different situations:

- During the transition between two consecutive spots when their distance was greater than $2cm$
- During the transition from one cluster to other.

The first situation is the same situation considered at CNAO. For the second situation it was implemented the clustering algorithm *bwlabel* from Matlab®.

The *bwlabel* is an image processing function that receives as input a binary image and returns a matrix containing labels of the connected objects (clusters) in the input [Mat12]. The labelling starts from picking a pixel $b_{ij} = 1$ and assign a label to this pixel and its neighbours. Then, the neighbours of these neighbours are also labelled (except those that have already been labelled), and so on. When this process terminates, other pixel that has not been labelled yet is selected and the labelling process repeated (with a different label) until all the $b_{ij} = 1$ pixels in the image are labelled.

The spot distribution in each slice was converted into a binary image with a pixel size that is given by the distance between the two closets spots (e.g. Fig.2.13).

2.3 Clinical Implications

The effect of the scan path optimization was accessed by studying the effect on the number of particle delivered in each TP. To do this study it was necessary to define a set of several parameters: the beam intensity (I in $particles^{-1}$), beam speed, FWHM, spot distribution, scan path and number of particles (N_p) delivered to each spot. The CNAO's TPS provides all these informations, except the beam speed which was assumed to be constant during all the irradiation, with a value of $20ms^{-1}$ [1].

For each treatment plan, four different optimizations were considered, one with the original scanning path (provided by CNAO's TPS) and the ones obtained with SA, HyGA and HyGA with

[1] The maximum scan speed allowed by the equipment at CNAO is $20ms^{-1}$

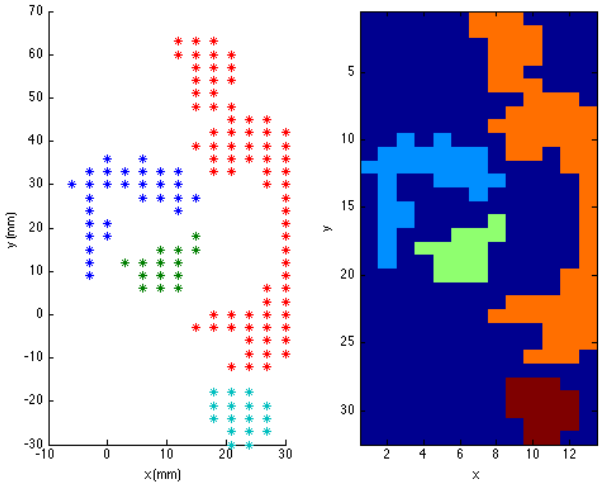

Figure 2.13: Cluster representation. On the left the spot distribution of one slice, each color represents one different cluster; on the right the respective image with a pixel size of $3mm \times 3mm$.

clustering.

The effect of the different optimization algorithms in the particles distribution was studied by considering a simple Pencil Beam Algorithm (section 1.1.5) and a water environment.

2.3.1 Coordinates system

Each slice was represented by a Cartesian grid ($x-y$ plane) positioned perpendicular along the beam axis ($z-axis$) (Fig.2.14a). The scan path of each slice was sampled and added to each 2D image matrix (Fig.2.14b). To each pixel corresponding to an irradiation spot it was assigned the correspondent value of prescribed particles. To each pixel corresponding to the transition between irradiation spots (the scanning path), the number of particles delivered was calculated by using the approximation 2.5. ΔQ is the distance between the center of two consecutive pixels, which was considered to be $1mm$.

$$N_P = \frac{I \times \Delta Q}{v \times 10^{-3}} \tag{2.5}$$

2.3.2 Pencil Beam Algorithm

By using the pencil beam algorithm, the dose delivered to each pixel can be calculated by using equation 1.4 in section 1.1.5. This equation can be divided into two terms: one representing the lateral dose contribution (Gaussian distribution) and the other related to the depth dose contribution.

Depth Dose Distribution In each treatment plan for a determined irradiation field there are N_s slices. Each slice is irradiated with a pencil beam whose energy is defined by the depth at each slice is. To each pencil beam with a different energy is associated a depth-dose curve (Fig.2.15).

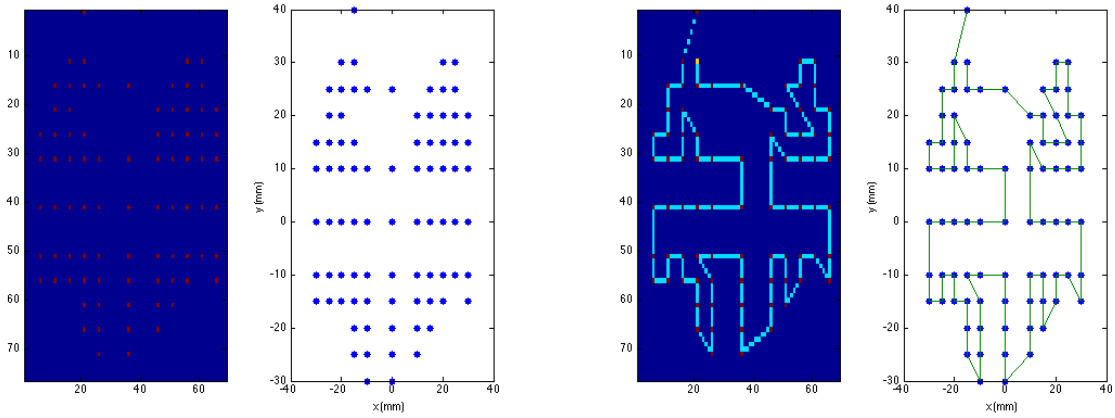

(a) On the left the image of the spot distribution on the right.

(b) On the left the image of the scan path on the right.

Figure 2.14: Spot distribution and path matrix.

Considering a slice i, the irradiation of the $N-i$ posterior slices [2] contributes to the dose distribution of the $1^{st}, 2^{nd} ... i^{th}$ slices. This dose contribution from each posterior slice is determined by the depth-dose curve of each pencil beam, the scanning path and spot distribution of each posterior slice. The depth-dose curves in water were obtained by Monte Carlo simulation [Cas12].

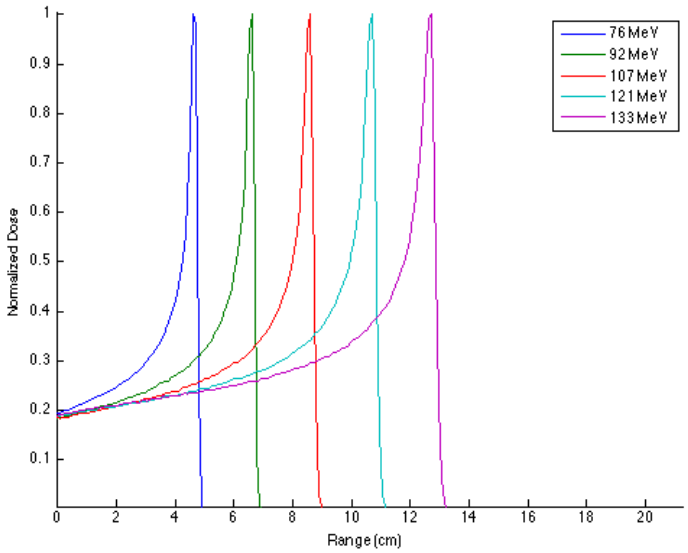

Figure 2.15: Depth-Dose Distribution profiles.

Lateral Dose Distribution As previously mentioned, the lateral dose distribution of a proton beam can be approximated to a Gaussian distribution. The *standard deviation*,σ, is calculated by using equation 2.6:

[2] slices irradiated with higher energies

$$\sigma = \frac{FWHM}{2\sqrt{2ln2}} \tag{2.6}$$

For every pixel of interest it was defined a polar grid (perpendicular to the $z - axis$) with radius of 3σ [HGB$^+$96]. This polar grid contained the lateral weights/contribution of the pencil beams irradiating each pixel - Gaussian matrix. The total lateral dose distribution of each slice was obtained by convolving the Gaussian matrix with each 2-D image matrix containing the irradiation spots and scanning path of each slice.

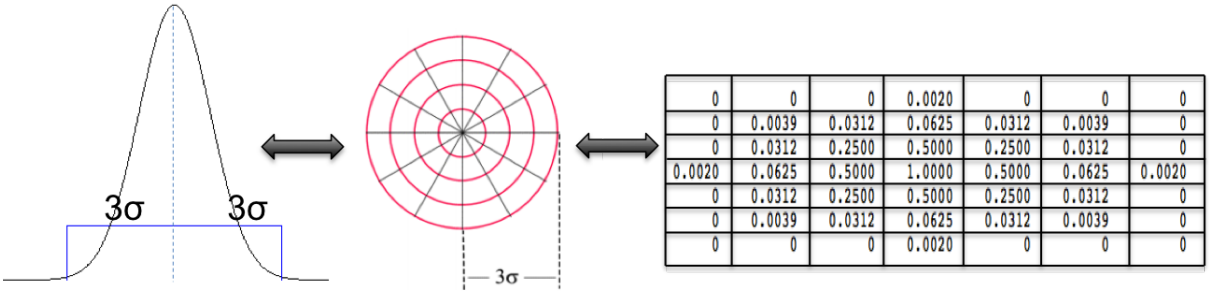

0	0	0	0.0020	0	0	0
0	0.0039	0.0312	0.0625	0.0312	0.0039	0
0	0.0312	0.2500	0.5000	0.2500	0.0312	0
0.0020	0.0625	0.5000	1.0000	0.5000	0.0625	0.0020
0	0.0312	0.2500	0.5000	0.2500	0.0312	0
0	0.0039	0.0312	0.0625	0.0312	0.0039	0
0	0	0	0.0020	0	0	0

Figure 2.16: On the left the normalized Gaussian distribution for a FWHM = 2, on the center the polar grid [Ǵ1] and on the right the 2D matrix with the weights of the polar grid - Gaussian matrix.

3

Results

All the data processing was done with Matlab® and using information from ten different treatment plans of CNAO's patients. Due to the large number of data ($\geq$ 3000 scan paths), only some results obtained for individual slices and the average values were selected to be shown. In appendix A, it is shown the results obtained in each individual treatment plan.

3.1 Genetic Algorithms Performance

In order to access the performance of each GA algorithm with different crossover (CX, OX, PMX) and mutation (random swap and GSTM) methods and the HyGA (section 2.1.3), it was calculated the scan path of two different slices. The evolution of the path length with the number of iterations is shown in Fig.3.1 and Fig.3.2.

The parameters considered in the simulations are in table 2.1 (section 2.1.4.1) and table 3.1. The population size, N_{pop} (Fig.2.3 and 2.10) was set to 30 individuals for slices with more than 30 irradiation spots, while for slices having lower or equal than 30 irradiation spots was set to the number of irradiation spots in the current slice.

For the GSTM method, the neighbourhood's size in the GSTM method (Fig.2.6 and 2.8a in section 2.1.4.1) was set to 2 when the number of irradiation spots in a slice was lower than 15 and to 5 when the number of spots was equal or higher than 15. The sub-tours were randomly selected with a random size between 2 and $\sqrt{N}$ (with N being the number of irradiation spots). The ε parameter in the HyGA (Fig.2.10) was set to the minimum distance between two consecutive spots in a scan path.

Fig.3.1a and Fig.3.2a show the spot distribution of the considered slices. The swap mutation method was tested with a CX crossover method (figures 3.1b and Fig.3.2b) against the GSTM with a CX crossover (figures 3.1c and 3.2c). The performance of the different crossover methods (CX, PMX and OX) was studied considering the GSTM method (figures 3.1c,3.1d,3.1e and figures 3.2c,3.2d,3.2e). In Fig.3.1f and Fig.3.2f it is shown the convergence (or evolution of the

path length with the number of iterations) of the HyGA method.

Table 3.1: Variables that are relevant for the GA.

Symbol	Definition	Value
P_c	Crossover probability	0.9
P_m	Mutation probability	0.2
P_i	Percentage of improvements	20%
P_e	Percentage of eliminations	30%
N_{it}	Number of iterations	50000
SP	Selective pressure	1.2

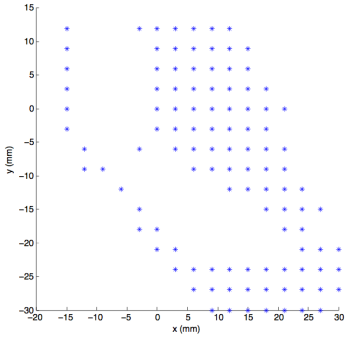

(a) Spot distribution

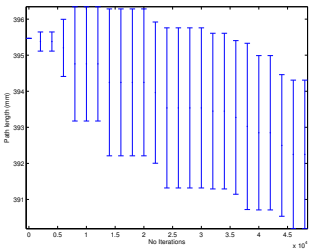

(b) CX with Swap mutation

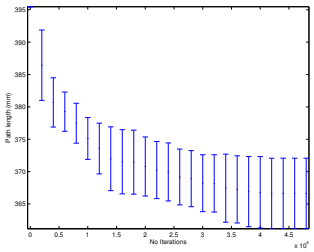

(c) CX with GSTM

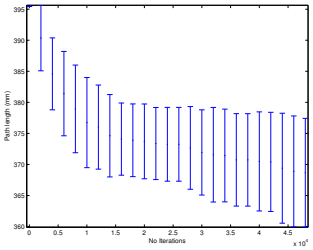

(d) PMX with GSTM

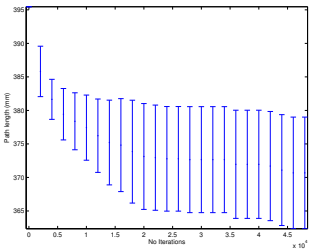

(e) OX with GSTM

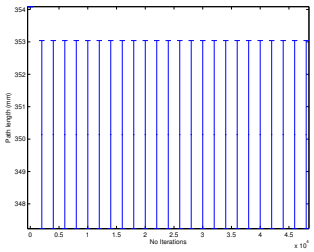

(f) HyGA

Figure 3.1: Convergence of GA using different crossover and mutation methods. Data show the average value and the standard deviation (error bar) of 10 runs. The slice contains 109 irradiation spots.

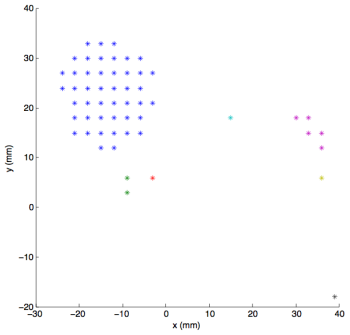

(a) Spot distribution

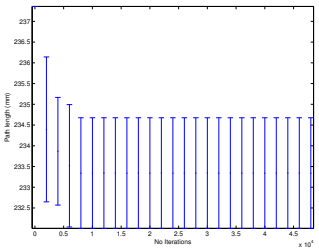

(b) CX with Swap mutation

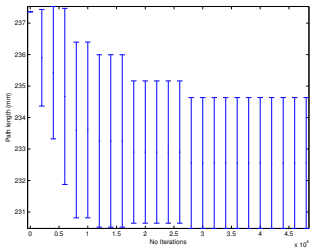

(c) CX with GSTM

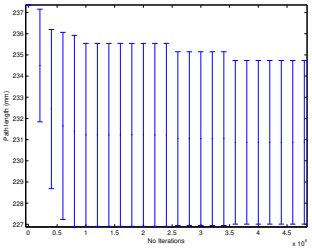

(d) PMX wit GSTM

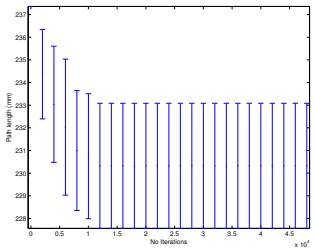

(e) OX with GSTM

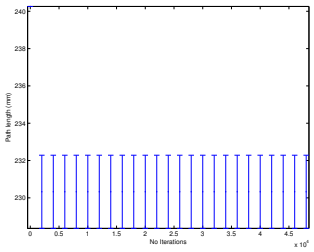

(f) HyGA

Figure 3.2: Convergence of GA using different crossover and mutation methods. Data show the average value and the standard deviation (error bar) of 10 runs. The slice contains 56 irradiation spots.

3.2 Scan Path Optimizations

From Fig. 3.3 to Fig. 3.6 if is shown different scan paths of four different slices. The optimization of the scan paths was performed using the SA (section 1.2.2), the HyGA (section 2.1.4.2) and the CNAO's TPS. The optimization parameters were the same as described in section 3.1, except the number of iterations, N_{it}, for the HyGA, which was set to 100. These slices were selected from all the data because they showed different spot patterns. The spot pattern can be considered uniform or non-uniform. A non-uniform slice contains more than one cluster of spots. The clusters of these slices are represented by different colors in the (d) figure of each one of the examples. The clusters were calculated using the clustering method proposed in section 2.2. This clustering method was coupled with the HyGA, performing independently the scan path optimization of each cluster, not taking into account their connection.

Fig. 3.7 and Fig. 3.8, show the average path length improvement as a function of the number of spots and clusters that can be found in the 10 treatment plans. Positive improvements (values above the line) represent a path $X\%$ shorter than the CNAO's TPS. While negative improvements (values under the line) represent path lengths $X\%$ longer than the CNAO's TPS. $X\%$ is the value given by the $y - axis$.

In table 3.2, it is shown the average path length travelled by the irradiation beam in a complete treatment plan and the relative difference between the path length of each one of the proposed optimization algorithms and the CNAO's TPS. The negative relative differences represent that the proposed methods (SA, HyGA and HyGA with clustering) obtained an average path length shorter than the CNAO's TPS.

The improvement (positive or negative) in the irradiation time can be considered the same as the path length improvement. For this it is necessary to consider a constant beam's speed and that no repainting of a slice is performed.

The individual results obtained from the optimization of each treatment plan can be viewed in appendix A.1, Fig. A.1 to Fig.A.10.

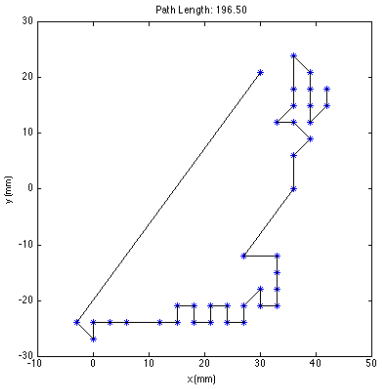

(a) CNAO's TPS

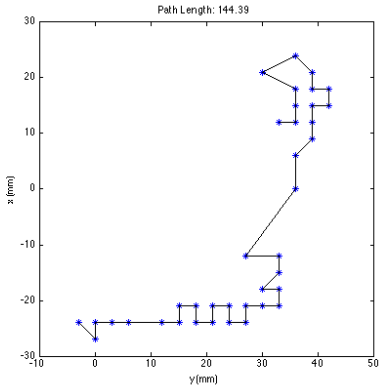

(b) HyGA scan path, $N_{it} = 100$

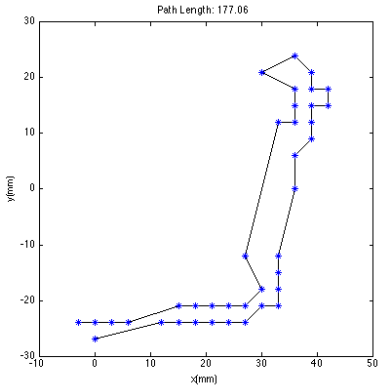

(c) SA scan path

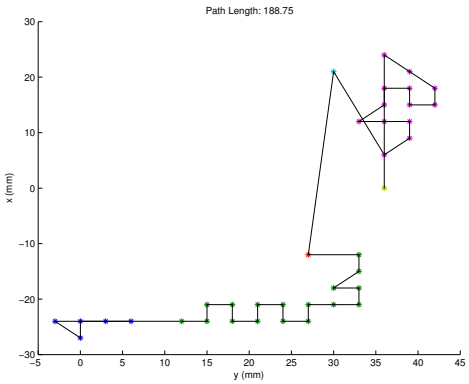

(d) HyGA with clustering, 6 clusters

Figure 3.3: Scan paths obtained with different optimization algorithms. The total path length is in mm..

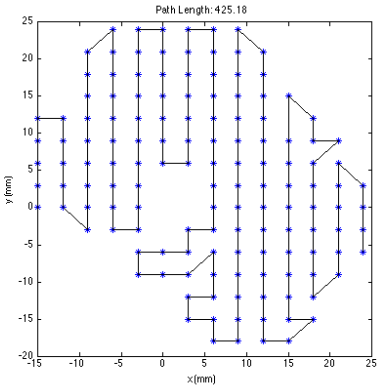

(a) CNAO's TPS

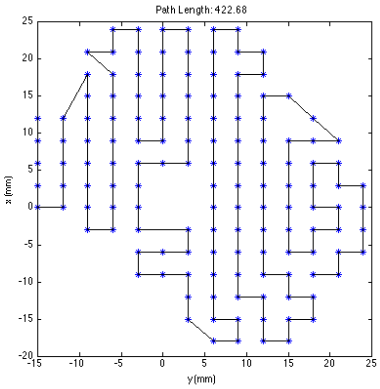

(b) HyGA scan path, $N_{it} = 100$

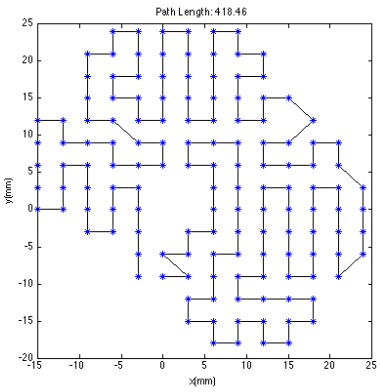

(c) SA scan path

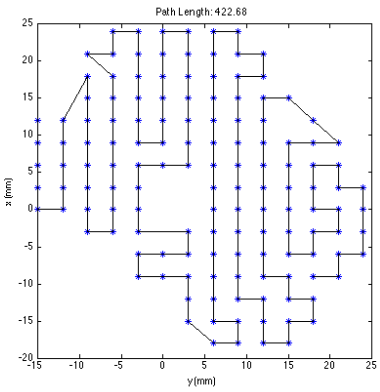

(d) HyGA with clustering, 1 cluster

Figure 3.4: Scan paths obtained with different optimization algorithms. The total path length is in mm..

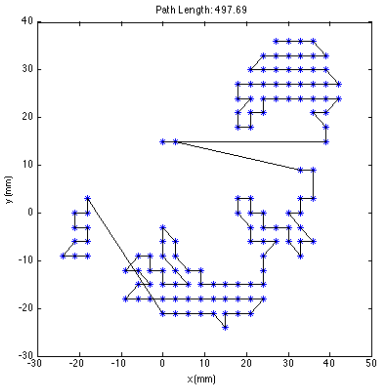

(a) CNAO's TPS

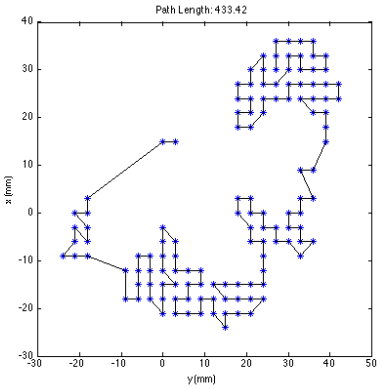

(b) HyGA scan path, $N_{it} = 100$

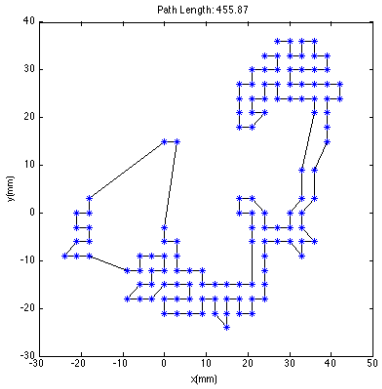

(c) SA scan path

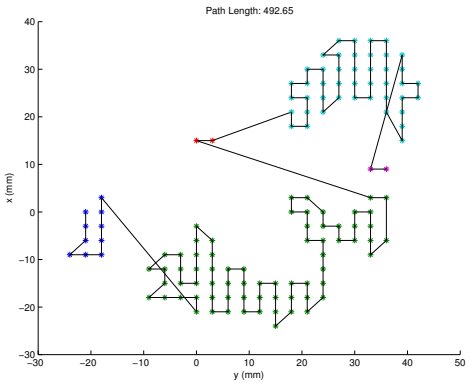

(d) HyGA with clustering, 5 cluster

Figure 3.5: Scanning paths obtained with different optimization algorithms. The total path length is in mm.

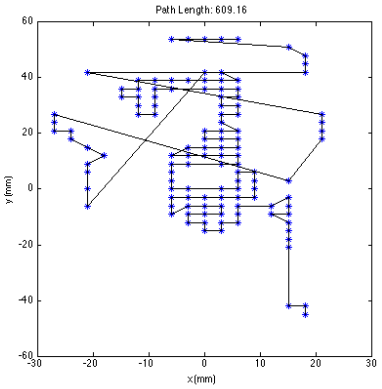

(a) CNAO's TPS

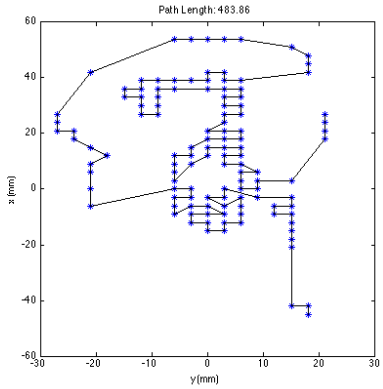

(b) HyGA scan path, $N_{it} = 100$

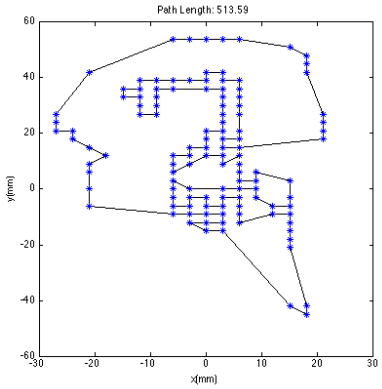

(c) SA scan path

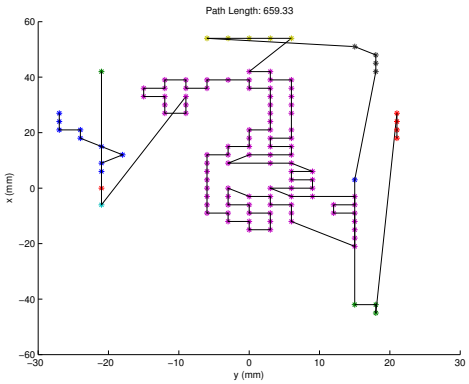

(d) HyGA with clustering, 10 cluster

Figure 3.6: Scanning paths obtained with different optimization algorithms. The total path length is in mm.

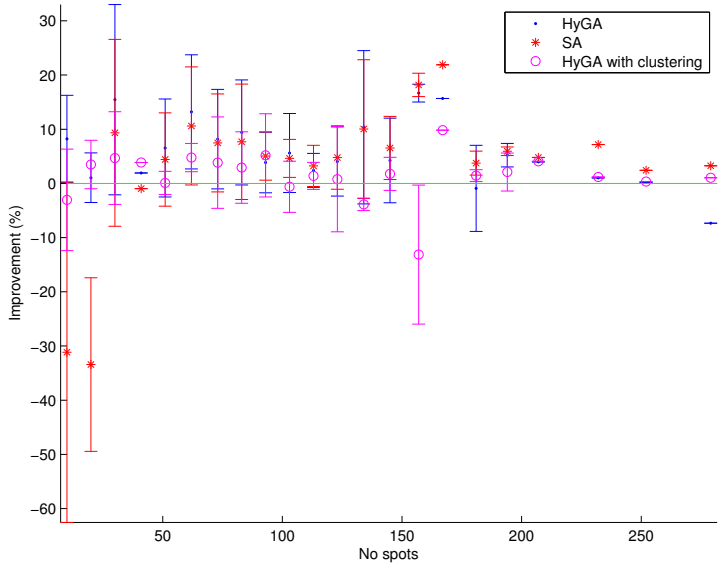

Figure 3.7: Average path length improvement as a function of the number of spots. The error bars are the standard deviation. For a given algorithm, a positive improvement value represents a shorter path than the CNAO's TPS. While a negative value represents a longer path.

Table 3.2: Average path length travelled in a complete TP. The relative difference is between the value obtained with the proposed methods and the value obtained with the CNAO's TPS. A negative relative difference value represents the perceptual reduction in the path length obtained with the CNAO's TPS.

Algorithm	Average path length	Relative difference (%)
CNAO's TPS	2.98E+04	-
Simulated Annealing	2.77E+04	-7.09
HyGA	2.74E+04	-8.05
HyGA with Clustering	2.93E+04	-1.84

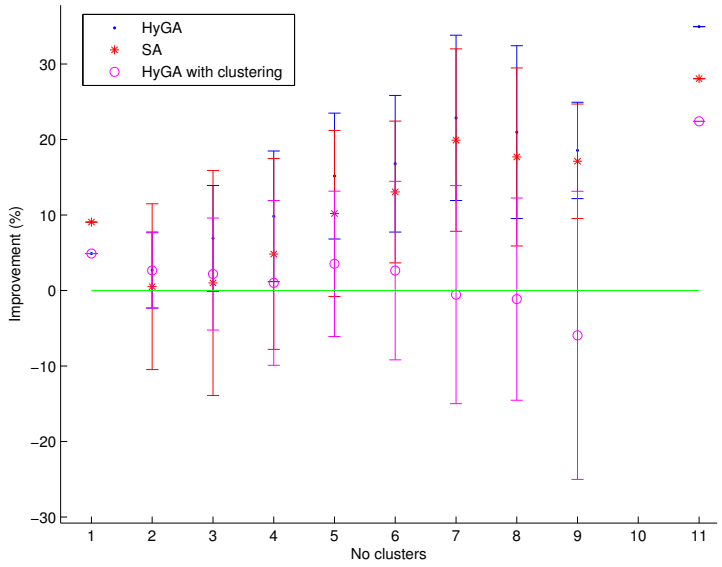

Figure 3.8: Average path length improvement as a function of the number of clusters. The error bars are the standard deviation. For a given algorithm, a positive improvement value represents a shorter path than the CNAO's TPS. While a negative value represents a longer path.

3.3 Clinical Implications

In this section it is presented the relevant results that measure the clinical implications of using the different optimization algorithms: SA, HyGA, HyGA with clustering and CNAO's TPS.

The quantitative effect of the scan path on the particle distribution was study in 3D, because the beam associated with a given spot does not only contribute to the dose of that slice but also delivers a dose to the more proximal slices. However, a 2D representation is useful to understand the effect of a specific scan path on the particle distribution in the slice. This effect can be viewed in Fig.3.9 and Fig.3.10 where it is shown the relative difference between the reference distribution of particles, evaluated assuming that no particles were delivered between irradiation spots, and those obtained with the CNAO's TPS, HyGA, SA and HyGA with clustering algorithms (i.e. the particles delivered during the path transition). The distributions were evaluated on a grid with $1mm \times 1mm$ pixel size. Each one of the distributions was obtained considering the use of chopper for spot transitions greater than $2cm$ for the CNAO's TPS, SA and HyGA. While for the HyGA the cluster was used during the transition between clusters.

Table 3.3 shows the average number of particles wasted due to the use of chopper. The particles wasted were calculated taking into account the beam intensity and the distance travelled by the beam while the chopper was being used. Table 3.4 shows the average number of particles delivered in a treatment plan, during the transition between irradiation spots. The number of particles delivered to each irradiation spot was not taken into account since was the same for all the optimization methods. Table 3.5 contains the average number of times the chopper was used for each one of the optimization methods.

The individual results about the number of particles wasted and delivered for each treatment plan can be viewed in appendix A.2.

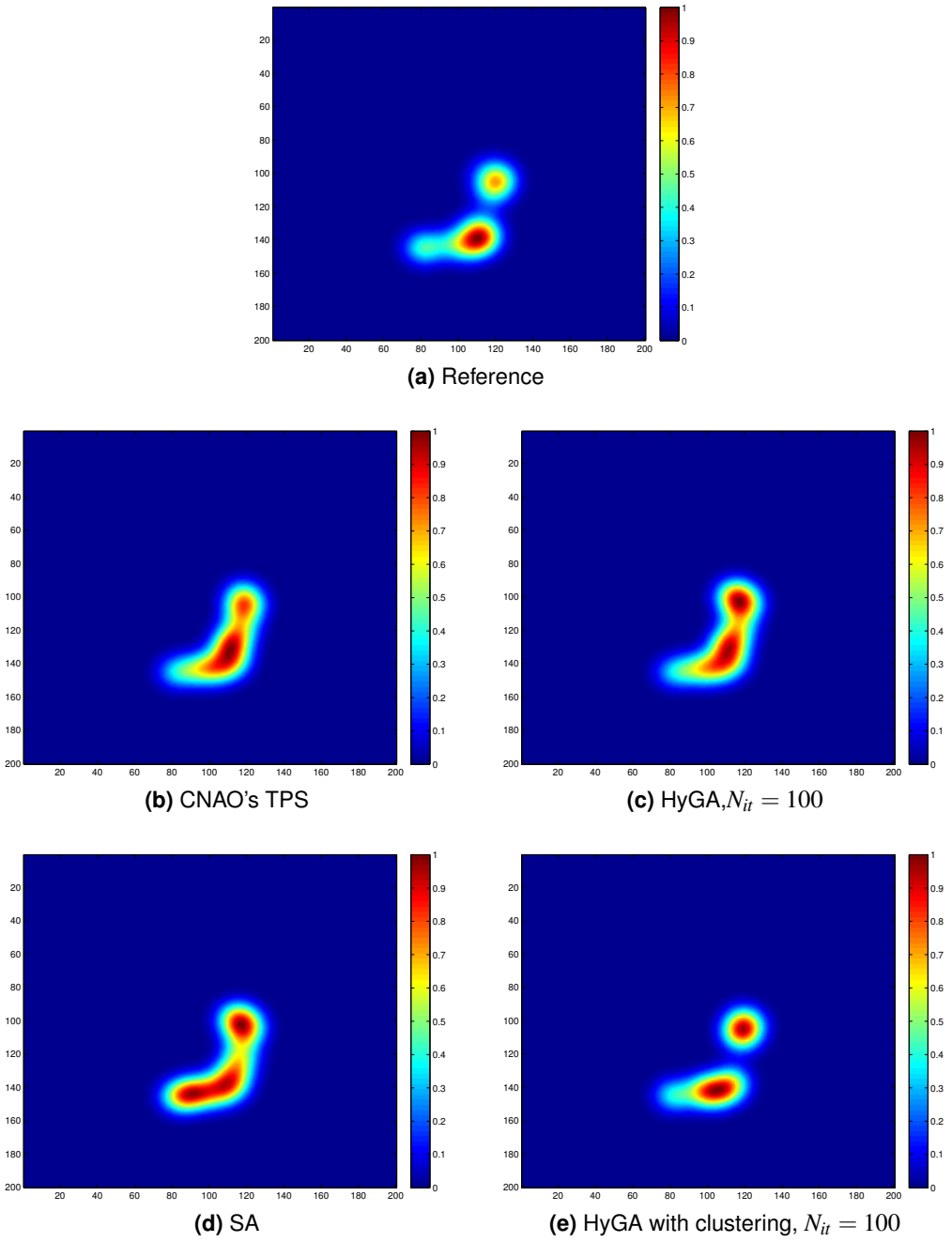

(a) Reference

(b) CNAO's TPS

(c) HyGA,$N_{it} = 100$

(d) SA

(e) HyGA with clustering, $N_{it} = 100$

Figure 3.9: Relative relative difference of particle distribution for the slice in Fig.3.3, using different optimization algorithms. (a) is the normalized particle distribution of the slice, considering that no particles are delivered during the spot transitions. The other sub-figures are the relative differences using the different optimization methods.(c) has 10% more particles than (b) in the path; (d) has 20% more particles than (b) in the path and (e) has 37% less particles than (b) in the path.

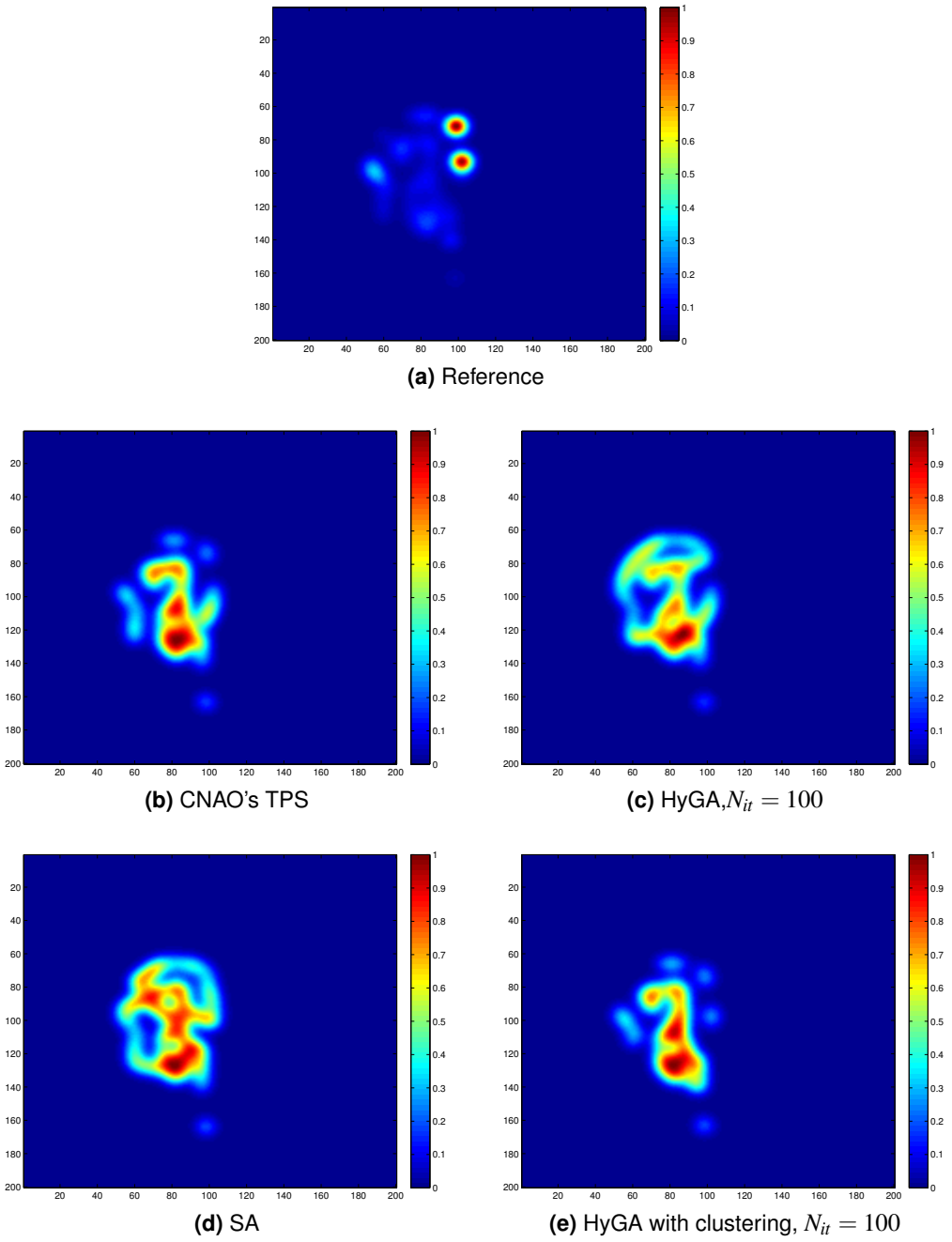

(a) Reference

(b) CNAO's TPS

(c) HyGA,$N_{it} = 100$

(d) SA

(e) HyGA with clustering, $N_{it} = 100$

Figure 3.10: Relative relative difference of particle distribution for the slice in Fig.3.6, using different optimization algorithms. (a) is the normalized particle distribution of the slice, considering that no particles are delivered during the spot transitions. The other sub-figures are the relative differences using the different optimization methods. (c) has 37% more particles than (b) in the path; (d) has 34% more particles than (b) in the path and (e) has 10% less particles than (b) in the path.

Table 3.3: Average particles wasted ($\mathbf{P_{wasted}}$) due to the use of chopper, in a complete TP. The relative difference is between the value obtained with proposed methods and the value obtained with the CNAO's TPS. A negative relative difference value represents the perceptual reduction in the number of particles wasted with the CNAO's TPS.

Algorithm	Average P_{wasted}	Relative difference (%)
Treatment Plan System	1.39E+08	-
Simulated Annealing	1.88E+07	-86.49
HyGA	9.08E+06	-93.46
HyGA with Clustering	1.96E+08	40.95

Table 3.4: Average particles delivered ($\mathbf{P_{Delivered}}$) during the transition between irradiation spots, in a complete TP. The relative difference is between the value obtained with the proposed methods and the value obtained with CNAO's TPS. A negative relative difference value represents the perceptual reduction in the number of particles delivered with the CNAO's TPS.

Algorithm	Average $P_{Delivered}$	Relative difference (%)
CNAO's TPS	6.86E+13	-
Simulated Annealing	7.07E+13	3.00
HyGA	7.24E+13	5.49
HyGA with Clustering	6.75E+13	-1.61

Table 3.5: Average number of times the chopper is used ($\mathbf{N_{chopper}}$), in a complete TP. The relative difference is between the value obtained with proposed methods and the value obtained with CNAO's TPS. A negative relative difference value represents the perceptual reduction in number of times the chopper is used with the CNAO's TPS.

Algorithm	Average $N_{chopper}$	Relative difference (%)
CNAO's TPS	81	-
Simulated Annealing	18	-77.79
HyGA	10	-87.22
HyGA with Clustering	200	148.64

3.4 Optimization tool

It was developed an optimization tool using Matlab® (Fig.3.11) that is able to read the treatment plan information and perform the scan path optimization of each slice.

The scan path optimization can be made using the CNAO's TPS, the SA, the HyGA and the HyGA with clustering. In Fig.3.11, it is shown the layout of the developed tool. This tool allows the possibility to select and compare the two scan paths obtained with two different optimization methods. This comparison considers the total path length in a given slice, the total number of particles wasted due to the use of chopper and the number of times it is used and the simulation time (Fig.3.12).

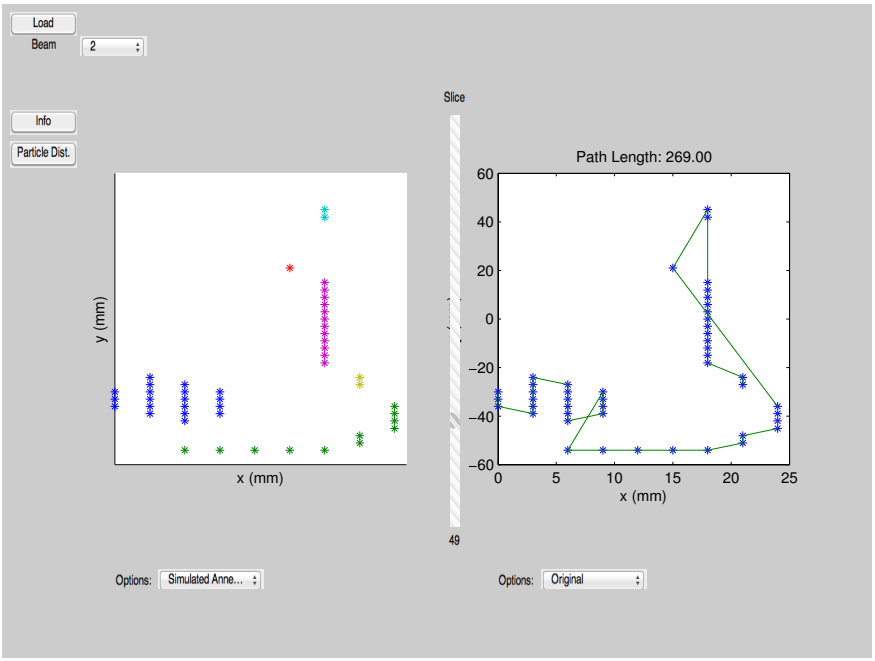

Figure 3.11: Layout of the optimization tool. Optimization tool that is able to read the patient's treatment plan information. The tool shows the different energy slices and offers the possibility to select which optimization algorithm should be used to calculate the scan path. Currently in the left subplot it is shown the spot pattern in a slice, while in the right subplot it is shown the path optimization with the CNAO's TPS.

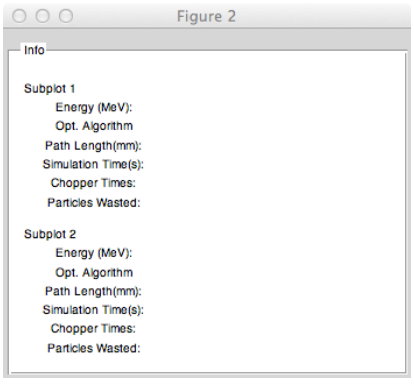

Figure 3.12: Optimization tool: information that is displayed about the scan path optimizations.

4

Discussion

4.1 Genetic Algorithms Performance

Section 3.1 shows the evolution of the path length as a function of the number of iterations, for the methods proposed in section 2.1.3. These results were obtained by calculating the scan path of two different slices, one with 109 spots and one cluster and other with 56 irradiation spots and 5 clusters.

For the first slice, (Fig.3.1) only the HyGA method converged (Fig.3.1f) to a possible solution. For the other methods the number of iterations considered was not enough for a convergence to a solution. In the second case (Fig.3.2) the OX with GSTM and the HyGA converged to a solution. However, the HyGA achieved the same solutions in less iterations, i.e. it presented a faster convergence.

Analysing figures 3.1b and 3.1c and figures 3.2b and 3.2c, where the swap mutation method was tested against the GSTM method, one can notice that the hybrid method offered the fastest convergence and best solutions than the swap mutation method.

The reason behind the fact that the hybrid methods (HyGA and the GA with GSTM) offered a faster convergence and better solutions is because during each iterations the algorithms try to improve the path.

Given these results the HyGA was selected for comparison with the other optimization methods (the SA and the CNAO's TPS).

4.2 Scan Path Optimizations

Analysing the total path length of each slice in section 3.2 (Fig.3.3 to Fig.3.6), it is possible to observe that both the HyGA and SA were able to produce scan paths shorter than the CNAO's TPS (form 0.6% to 27 %). This path length improvement is more pronounce in figures 3.3,3.5 and 3.6 than in Fig.3.4. Examining these paths and the results shown in Fig.3.8, one can observe

that the path length reduction is more significant when the optimization is performed for slices with several clusters of spots. Also, by Fig.3.4 one can observe that the optimization of the scan path for slices with an uniform and compact distribution (smaller number of clusters) yields little or no benefit from the CNAO's TPS.

Examining figures 3.3, 3.5 and 3.6, it is possible to notice that the HyGA and the SA avoid crossings in the path and the irradiation of "holes" (vacancies in the spot pattern). Since in *quasidiscrete scanning* the beam is never turned off, the presence of crossings in the path may lead to the creation of hot spots. Moreover, in the case of organs at risk where the vacancies in the spot pattern are located, it may be important to ensure that the beam is either turned off or that the path is optimized to avoid these regions and crossings in the path. Therefore, at CNAO it is used the chopper, which as previously mentioned, is a device that avoids the irradiation of a slice when the transition between two consecutive spots is greater than $2cm$.

In order to take advantage of the utilization of the chopper, it was implemented a clustering algorithm (section 2.2) with the HyGA. By using the clustering algorithm the spot pattern was divided into clusters and the path optimization of each cluster was made independently. The connection between clusters was not optimized, which led to longer scan paths, crossings and irradiation of "holes" in figures 3.3,3.5 and 3.6. However, these is not relevant in terms of dose delivered to the patient because the chopper will be used between the cluster transitions.

Figures 3.7 and Fig.3.8 show the average path improvement in ten treatment plans, as a function of the number of spots and the number of clusters, respectively. As previously mention, positive values represent an improvement in the path length. As one can notice, the SA method does not offer shorter paths for slices with lower number of spots ($\approx\leq 40$), while for larger number of spots ($\approx\geq 150$) in a slice is the method that offers the best results (Fig.3.7 and Fig.A.1 to Fig.A.10). For the HyGA the opposite is verified. The reason behind this fact is maybe because the SA's parameters were set to values that according to Pardo, *et al.*[PDB$^+$09] were calculated to take full advantage of the algorithm. The selection of the HyGA's parameters was not properly study.

Table 3.2 shows the average path length travelled per treatment plan and the relative difference between the CNAO's TPS and each one of the optimization algorithms. On average, all optimization methods, SA, HyGA and HyGA with clustering, were able to improve the total path length (7%,8% and 2% respectively). However, this improvement was not very significant due to the fact that in a 3-D model there are different types of slices, with uniform and non-uniform spot patterns. If one considers individual slices the improvement can go to more than 30% (Fig.A.1 and Fig.A.8 in appendix A).

The reduction in the irradiation time, not considering repainting and considering that the use of the chopper does not influences the irradiation time, is the same as the path length reduction. For instance, for the average path lengths in table 3.2 (not considering the time spent in changing

the energy and the stops in each irradiation spots for delivering the prescribed particles) the scanning time is 0.68, 0.63, 0.62 and 0.67 seconds (for $20ms^{-2}$ beam speed) for the CNAO's TPS, SA, HyGA and HyGA with clustering respectively. The improvement would be in the order of some milliseconds which would not be detected by the patient, making not relevant the study of the treatment time improvement.

The simulation time was also not taken into account due to the fact that different programming languages were used (C++ and Matlab®). However, the HyGA clustering algorithm offers the advantage of parallel simulations (independent optimization of the clusters).

4.3 Clinical Implications

In Fig.3.9 and Fig.3.10) it is shown the relative difference between the reference distribution and the those obtained with the CNAO's TPS, SA, HyGA and HyGA algorithms. As it is visible in these figures, the HyGA with clustering presented a smaller irradiation area than the other methods. This is due to the fact that between cluster transitions the chopper was used, avoiding the irradiation of "holes" in a slice.

Table 3.4 shows that, on average, only the HyGA has led to less particles delivered in the scan path than the CNAO's TPS (about 2% less). However, the number of particles wasted in the chopper was, on average, about 41% higher than the CNAO's TPS (table 3.3).

For the SA and HyGA, the number of particles wasted with the CNAO's TPS was reduced in about 86% and 93%. However, the number of particles delivered in the scan path was about 3% and 5% higher. The number of particles delivered in the path with the HyGA was higher than for the SA because, as it is possible to see in figures 3.3,3.5 and 3.6, this algorithm tries to minimize longer transitions between irradiation spots, reducing the number of times the chopper is used (table 3.5).

The number of times the chopper was used (table 3.5) and the particles wasted due to its utilization (table 3.3) can be used as a measure of the energy spent by the treatment plan equipment, because it makes the accelerator to produce a higher number of particles (due to longer scan paths) and not delivering them.

4.4 Final Discussions

To sum up, given the previous results, each one of the optimization algorithms (CNAO's TPS, SA, HyGA and HyGA with clustering) presented advantages and disadvantages. Considering the path optimization, in the case of uniform patterns (1 cluster) and/or high number of spots in a slice (on average ≥ 200 spots), the SA was able to improve the path length, while for

non-uniform distributions this was better accomplished by the HyGA. Considering the clinical implications of the optimization algorithms, the SA and HyGA showed to be the most energy efficient, since the number of particles wasted was considerably decrease. However, the CNAO's TPS and the HyGA with clustering were the methods that showed an lower amount of delivered particles unnecessary to the patient. Taking into account these results, the developed tool was implemented considering all these optimization algorithms (SA, HyGA, HyGA with clustering and CNAO's TPS), allowing the selection of which algorithm is used.

The path optimization should be more relevant for facilities where the *quasidiscrete scanning* without chopper is used. This is due to the fact that in this situations the number of particles delivered to the patient is proportional to the path length, making essential an optimization algorithm that provides shorter paths and avoid irradiation of "holes" in a slice. Taking into account these conditions the SA and HyGA would present an advantage because they were able to obtain shorter paths.

5

Conclusion

In *active scanning* path optimization is crucial to reduce the treatment time, the energy used by the treatment equipment and the dose delivered between the irradiation spots (extra dose). We sought to study the effect of different optimization algorithms on the scan path and their implications in a clinical environment. The optimization algorithms used were Simulated Annealing (SA) and Genetic Algorithms.

The performance of different genetic algorithm methods were studied, leading to the selection of the Hybrid Genetic Algorithm with Heuristics (HyGA).

When compared with the HyGA, the SA presented longer paths for slices with non-uniform patterns and with a lower amount of irradiation spots. However, both algorithms showed that shorter paths were obtained than the ones calculated with the current CNAO treatment plan system (CNAO's TPS). This improvement was more pronounced for slices with non-uniform spot patterns.

In order to reduce the extra dose, CNAO uses a device called the chopper, which deflects the beam out of the extraction line when the distance between two consecutive irradiation spots is greater than $2\,\mathrm{cm}$. Access to the chopper has led to the development of the a HyGA with clustering. This algorithm took into consideration that the chopper was used every time there was a transition between clusters. This method was able to reduce, on average, the number of particles delivered with the CNAO's TPS by 2%.

One drawback of using the chopper is an increase in the number of particles wasted by the equipment. The SA and HyGA method were able to reduce, on average, the number of particles wasted by the CNAO's TPS by 86% and 93%, respectively. However, both these algorithms showed an increase of 3% and 5% in the number of particles delivered, compared to the CNAO's TPS.

Given these results, one can conclude that the proposed optimization algorithms can be useful for two different aims.

The first aim is the reduction in the energy spent by the treatment equipment. At CNAO, this

can be achieved by using the SA and HyGA methods, which significantly reduce the number of particles wasted due to the chopper's utilization. For a facility with *quaisdiscrete scanning* and without a chopper, the SA and HyGA provide shorter irradiation paths, saving energy from the magnets.

The second aim is the reduction in the dose delivered to the patient (which is related with the number of particles delivered). For the CNAO facility, this reduction can be achieved by using the HyGA method with clustering that, in some situations, offers a reduction of 13% (TableA.6) from the CNAO's TPS.

For future work, from a mathematical point of view the optimization parameters (such as crossover and mutation probability) should be studied in order to improve the performance of the optimization algorithms. From a clinical point of view, a study that evaluates the relevance of the dose delivered to the patient of the extra 3% and 5% particles delivered with the SA and HyGA can be performed.

To conclude, as mentioned, more work can be developed in this project. However, the proposed aims were fulfilled.

Bibliography

[AA11] M. Albayrak and N. Allahverdi. Development a new mutation operator to solve the traveling salesman problem by aid of genetic algorithms. *Expert Systems With Applications*, 38 issue 3:1313–1320, 2011.

[ADA08] Buthainah Al-Dulaimi and Hamza Ali. Enhanced traveling salesman problem solving by genetic algorithm technique (tspga). *World Academy of Science, Engineering and Technology*, 3, 2008.

[Ama01] Ugo Amaldi. The italian hadrontherapy project CNAO. *Physica Medica*, XVII, Supplement 1, 2001.

[AT91] Ugo Amaldi and G. Tosi. Per un centro di teleterapia con adroni. *TERA 1-1*, 1991.

[Att91] F. Attix. *Introduction to Radiological Physics and Radiation Dosimetry*. John Willey & Sons, 1991.

[Bry00] Kylie Bryant. *Genetic Algorithms and the Traveling Salesman Problem*. PhD thesis, Harvey Mudd College, 2000.

[Cas12] Inês Castelhano. Depth-dose distribution for active beam scanning in proton therapy. Internship Report, September 2012.

[CC09] Alexander W. Chao and Weiren Chou, editors. *Reviews of Accelerator Science and Technology, Volume 2, Medical Applications of Accelerators*. World Scientific, 2009.

[CER11] CERN. European organization for nuclear research. Online, November 2011. Available from: `http://public.web.cern.ch/public/`.

[CH06] Chao-Rong Chen and Sheng-Chyang Huang. The study of the longest non-intersecting route problem using genetic algorithm. *IEEE International Conference on Systems, Man, and Cybernetics*, 2006.

[CNA12] Fondazione CNAO. National handrotherapy center for cancer treatment. Online, August 2012. Available from: `http://www.cnao.it/en`.

[Cre05] Paulo Crespo. *Optimization of In-Beam Positron Emission Tomography for Monotoring Heavy Ion Tumor Therapy*. PhD thesis, Technische Universität Darmstadt, 2005.

[Dar59] C. Darwin. *The origin of species*. Murray, London, 1859.

[Dav85] L. Davis. Applying adaptive algorithms to epistatis domains. *Proceedings of the International Joint Conference on Artificial Intelligence*, 1985.

[Dav10] Donald Davendra, editor. *Traveling Salesman Problem, Theory and Applications*. InTech, 2010.

[Ǵ11] Joanna Góra. Wp13 – m2 first 3d dose computation. PARTNER, Grant Agreement Number 215840, March 2011. Available from: https://espace.cern.ch/partnersite/workspace/gora/Shared%20Documents/Milestone%202.pdf.

[GAA+08] S. Giodanengo, A. Ansarinejad, A. Attili, F. Bourhaleb, B. Cirio, M. Donetti, M. A. Garella, F. Marchetto, G. Mazza, V. Monaco, J. Pardo Montero, A. Pecka, G. Russo, and R. Sacchi. The CNAO system to monitor and control hadron beams for therapy. *IEEE Nuclear Science Symposium Conference Record*, 2008.

[GGKL05] Osvaldo Gervasi, Marina Gavrilova, Vipin Kumar, and Antonio Laganá, editors. *Computational Science and Its Applications - ICCSA 2005: Part IV*. Springer, 2005.

[GL85] D. E. Goldberg and R. Lingle. Alleles, Loci and the TSP. *Proceedings of the First International Conference on Genetic Algorithms*, 1985.

[Goe11] Marc Goetschalckx, editor. *Supply Chain Engineering*. Springer, International Series in Operations Reseach & Management Science, 2011.

[Goi08] M. Goitein. *A Physcist's Eye View*. Springer, New York, 2008.

[Gro05] By Sven Oliver Grozinger. Particle beam application: on the way to optimum dose conformity. *Science Particle Therapy, Medical Solutions*, 2005.

[Gro12] Particle Therapy Co-Operative Group. Particle therapy facilities in operation (incl. patient statistics). Online, August 2012. Available from: http://ptcog.web.psi.ch/ptcentres.html.

[GSI11] Helmholtzzentrum für Schwerionenforschung GmbH GSI. Chair. Online, December 2011. Available from: https://www.gsi.de/forschung/bio/chair_e.html.

[Hea11] Siemens Healthcare. Centro nazionale di adroterapia oncologica - CNAO. Online, November 2011. Available from: http://www.medical.siemens.com/webapp/wcs/stores/servlet/CategoryDisplay~q_catalogId~e_-11~a_categoryId~e_1033670~a_catTree~e_100010,1008643,1033666,1033668,1033670~a_langId~e_-11~a_storeId~e_10001.htm.

[HGB+96] Linda Hong, Michael Goitein, Marta Bucciolini, Robert Comiskey, Bernard Gottschalk, Skip Rosenthal, Chris Serago, , and Marcia Urie. A pencil beam algorithm for proton dose calculations. *Phys. Med. Biol.*, 41:1305Ð1330, 1996.

[HKM11] Yoshihiko Hatano, Yosuke Katsumura, and A. Mozumder, editors. *Charged Particle and Photon Interactions with matter, Recent Advances, Applications, and Interfaces*. CRC Press, Taylor & Francis Group, 2011.

[Hol75] J. H. Holland. Adaptation in natural and artificial systems. *University of Michigan Press*, 1975.

[IFT+07] Taku Inaniwa, Takuji Furukawa, Takehiro Tomitani, Shinji Sato, Koji Noda, and Tatsuaki Kanai. Optimization for fast-scanning irradiation in particle therapy. *Med. Phys.*, 34, 2007.

[KFM+10] A. Kitagawa, T. Fujita, M. Muramatsu, S. Biri, and A. G. Drentje. Review on heavy ion radiotherapy facilities and related ion sources (invited). *Rev. Sci. Instrum*, 2010.

[KWO07] Joanne H. Kang, Jan J. WilkensÍ', and Uwe Oelfke. Demonstration of scan path optimization in proton therapy. *Med. Phys*, 34, 2007.

[lab11] TBM lab. Laboratorio cart. Online, December 2011. Available from: `http://www.tbmlab.polimi.it/labs/cart/cart.htm`.

[Lin12] Ute Linz, editor. *Ion Beam Therapy*. Springer, 2012.

[LKM+99] P. Larranga, C.M.H. Kuijpers, R.H. Murga, I. Inza, and S. Dizdarevic. Genetic algorithms for the travelling salesman problem: A review of representations and operators. *Artificial Intelligence Review, Kluwer Academic Publishers*, 13:129–170, 1999.

[Mat12] Matlab®. Steve on image processing. Online, August 2012. Available from: `http://blogs.mathworks.com/steve/2008/03/25/bwlabel-search-order/`.

[Onc12] OncoLink. Proton therapy: The basics. Online, September 2012. Available from: `http://www.oncolink.org/treatment/article.cfm?id=433&s=70&c=9`.

[Org12] World Health Organization. Cancer. Online, September 2012. Available from: `http://www.who.int/mediacentre/factsheets/fs297/en/`.

[OSH87] I. M. Oliver, D. J. Smith, and J. R. C. Holland. A study of permutation crossover operators on the traveling salesman problem. *Proceedings of the Second International Conference on Genetic Algorithms on Genetic algorithms and their application*, 1987.

[OzR12] Factors influencing the oxygen effect. OzRadOnc, August 2012.

[Pag12] Harald Paganetti, editor. *Proton Therapy Physics*. CRC Press, Taylor & Francis Group, 2012.

[PDB+09] J. Pardo, M. Donetti, F. Bourhaleb, A. Ansarinejad, and et al. Heuristic optimization of the scanning path of particle therapy beams. *Med. Phys.*, 36, 2009.

[PG00] H. Paganetti and M. Goitein. Radiobiological significance of beam line dependent proton energy distributions in a spread-out bragg pe. *Med. Phys*, 2000.

[Pic11] M. Piccaluga. Meno pazienti da fuori regione, dea e CNAO carte per il rilancio. La Provincia Pavese, October 2011. Available from: http://laprovinciapavese.gelocal.it/cronaca/2011/10/29/news/meno-pazienti-da-fuori-regione-dea-e-cnao-carte-per-il-rilancio-1.1631207.

[PJP+08] Harald Paganetti, Hongyu Jiang, Katia Parodi, Roelf Slopsema, and Martijn Engelsman. Clinical implementation of full monte carlo dose calculation in proton beam therapy. *Phys. Med. Biol.*, 53:4825–4853, 2008.

[PK11] Seo Hyun Park and Jin Oh Kang. Basics of particle therapy i: physics. *Radiation Oncology Journal*, 29(3):135–146, 2011.

[PTVF07] William H. Press, Saul A. Teukolsky, William T. Vetterling, and Brian P. Flannery. *Numerical Recipes: The Art of Scientific Computing*. Cambridge University Press, 2007.

[Pul08] M. Pullia. Status report on the centro nazionale di adroterapia oncologica (CNAO). *Proceedings of EPAC08, Genoa, Italy*, 2008.

[RBE08] *Relative Biological Effectiveness in Ion Beam Therapy, Technical reports series No. 461*. International Atomic Energy Agency, 2008.

[Rob12] David Robin. An overview of next generation gantries. Online, July 2012. Available from: http://erice2011.na.infn.it/TalkContributions/Robin.pdf.

[SA07] Martin Soukup and Markus Alber. Influence of dose engine accuracy on the optimum dose distribution in intensity-modulated proton therapy treatment plans. *Phys. Med. Biol.*, 52:725–740, 2007.

[SEJS06] Daniela Schulz-Ertner, Oliver Jake, and Wolfgang Schlegel. Radiation therapy with charged particles. *Semin Radiat Oncol, Elsevier Inc.*, 2006.

[SFA05] Martin Soukup, Matthias Fippel, and Markus Alber. A pencil beam algorithm for intensity modulated proton therapy derived from monte carlo simulations. *Phys. Med. Biol.*, 50:5089–5104, 2005.

[SI93] H. Sengoku and I.Yoshihara. A fast tsp solver using ga on java. *Information Processing Society of Japan 46th Natĺ Conv*, 1993.

[sit12] Ionization and cell damage. NDT Resource Center, August 2012. Available from: http://www.ndt-ed.org/EducationResources/CommunityCollege/RadiationSafety/theory/ionization.htm.

[TER11] Tera foundation. Online, October 2011. Available from: www.tera.it.

[TLB+58] C. Tobias, J. Lawrence, J. Born, R. McCombs, J. Roberts, H. Anger, B. Low-Beer, and C. Huggins. Pituitary irradiation with high energy proton beams: A preliminary report. *Cancer Res*, 1958.

[Tur07] J.E. Turner. *Atoms, Radiation and Radiation Protection*. Wiley-VCH, 2007.

[Wik11a] Wikipedia. Centro nazionale di adroterapia oncologica. Online, October 2011. Available from: http://it.wikipedia.org/wiki/Centro_Nazionale_di_Adroterapia_Oncologica.

[Wik11b] Wikipedia. Genetic algorithm. Online, December 2011. Available from: http://en.wikipedia.org/wiki/Genetic_algorithm.

[Wik11c] Wikipedia. Simulated annealing. Online, December 2011. Available from: http://en.wikipedia.org/wiki/Simulated_annealing.

[Wik12a] Wikipedia. 2-opt. Online, July 2012. Available from: http://en.wikipedia.org/wiki/2-opt.

[Wik12b] Wikipedia. Travelling salesman problem. Online, September 2012.

[Wil46] R. Wilson. Radiological use of fast protons. *Radiology*, 1946.

[WK08] U Weinrich and C M Kleffner. Comissioning of the carbon beam gantry at the heidelberg ion therapy (hit) accelerator. *11th European Particle Accelerator Conference, Genoa, Italy,*, 2008.

A

Appendix

A.1 Scan Path Optimizations

In this section it is shown the path length improvement as a function of the number of spots and clusters that can be found in each treatment plan. Positive improvements (values above the line) represent a path X% shorter than the CNAO's TPS. While negative improvements (values under the line) represent path lengths X % longer than the CNAO's TPS. X % is the value given by the $y-axis$.

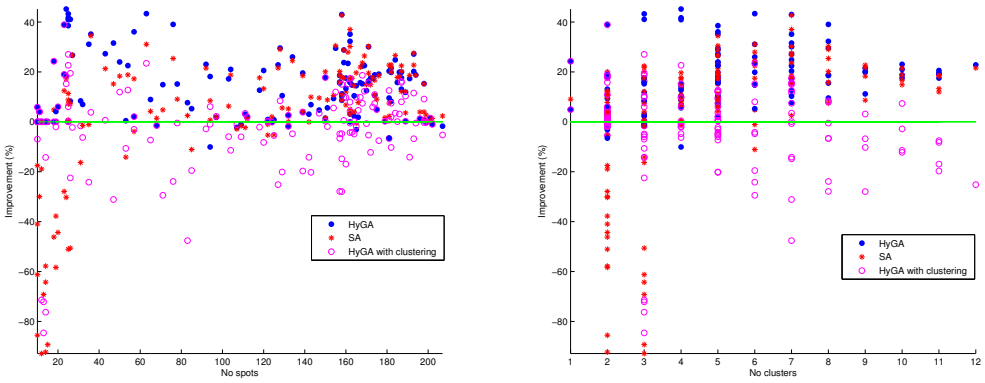

Figure A.1: Path length improvement, TP1. The improvement is shown as a function of the number of irradiation spots (left) and clusters (right) in a treatment plan.

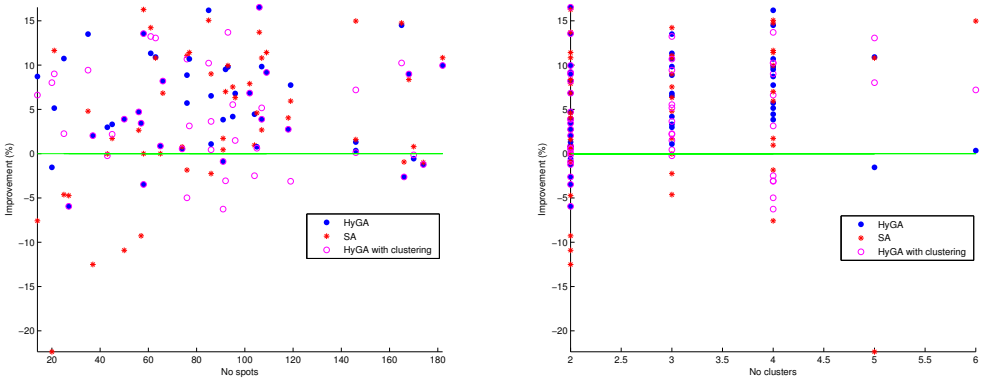

Figure A.2: Path length improvement, TP2. The improvement is shown as a function of the number of irradiation spots (left) and clusters (right) in a treatment plan.

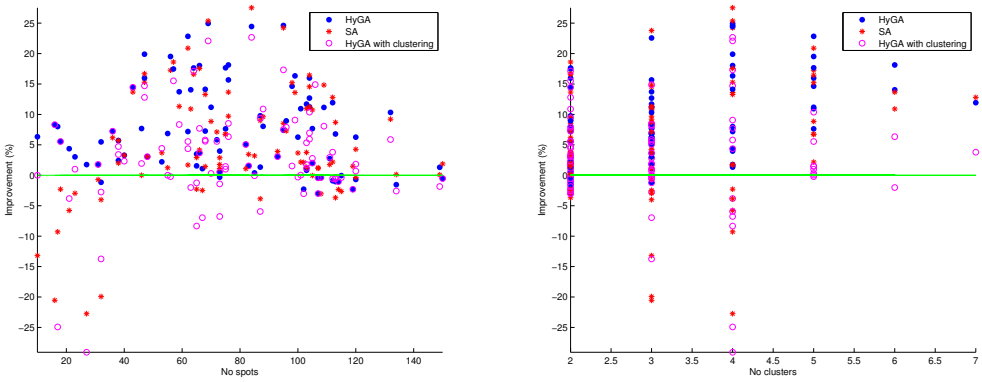

Figure A.3: Path length improvement, TP3. The improvement is shown as a function of the number of irradiation spots (left) and clusters (right) in a treatment plan.

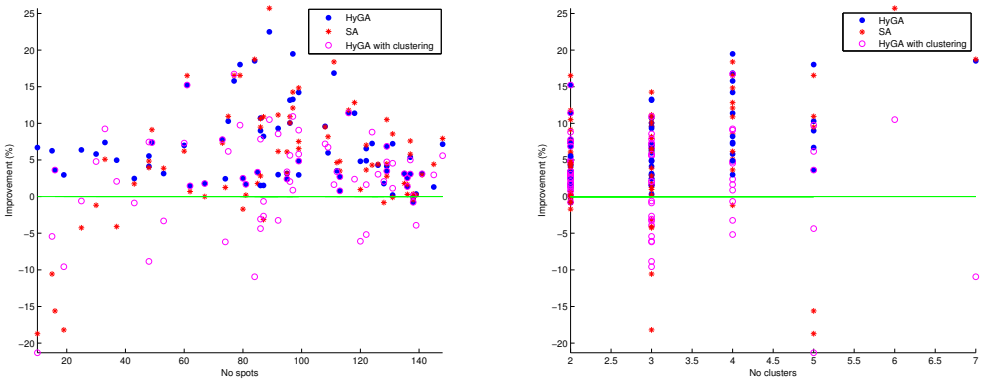

Figure A.4: Path length improvement, TP4. The improvement is shown as a function of the number of irradiation spots (left) and clusters (right) in a treatment plan.

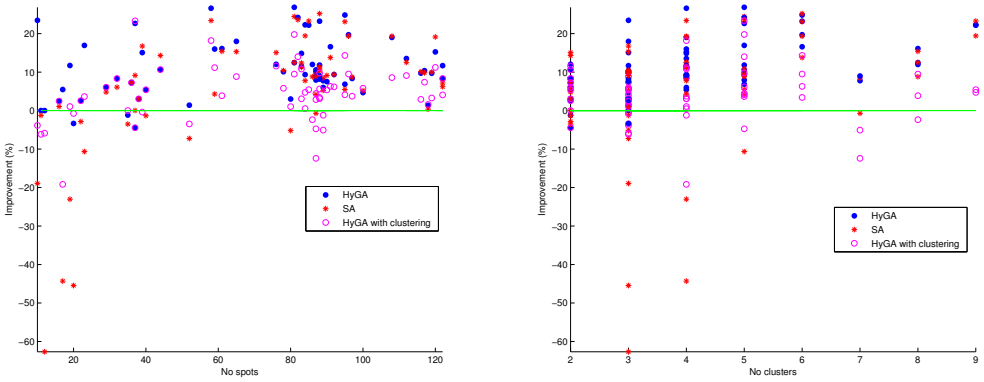

Figure A.5: Path length improvement, TP5. The improvement is shown as a function of the number of irradiation spots (left) and clusters (right) in a treatment plan.

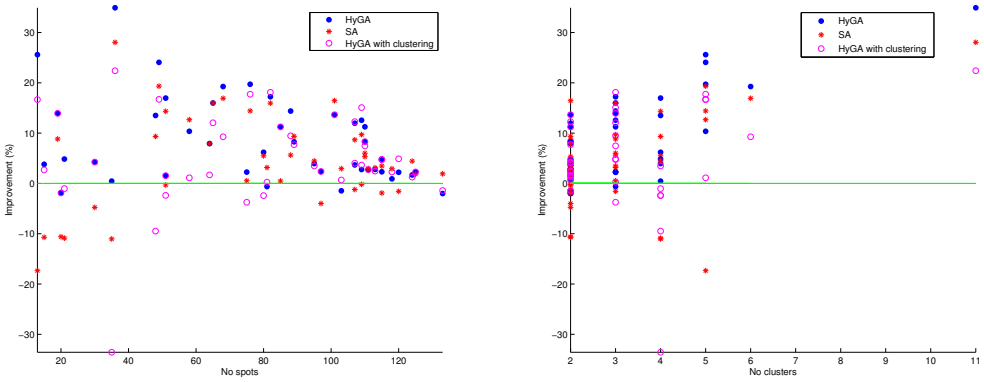

Figure A.6: Path length improvement, TP6. The improvement is shown as a function of the number of irradiation spots (left) and clusters (right) in a treatment plan.

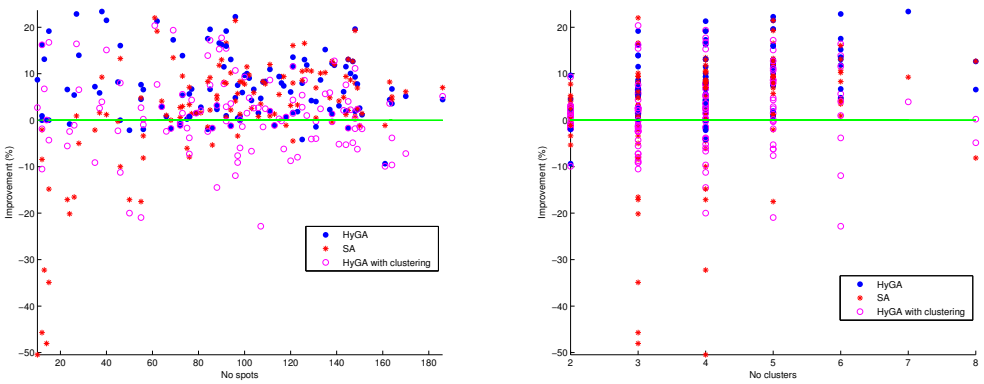

Figure A.7: Path length improvement, TP7. The improvement is shown as a function of the number of irradiation spots (left) and clusters (right) in a treatment plan.

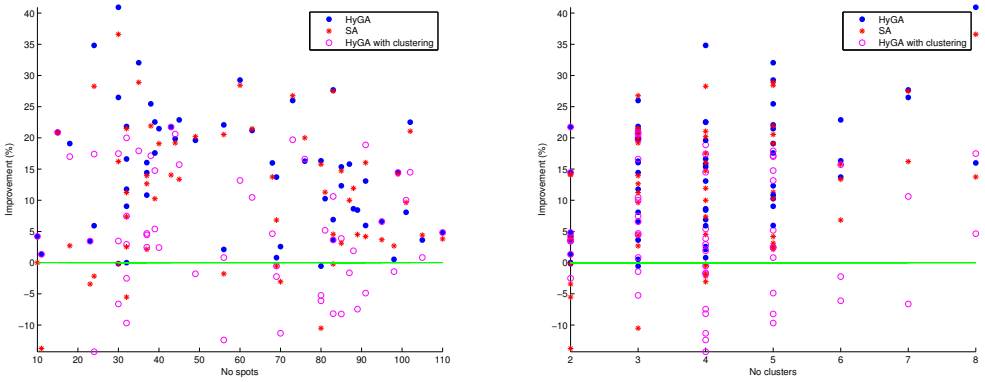

Figure A.8: Path length improvement, TP8. The improvement is shown as a function of the number of irradiation spots (left) and clusters (right) in a treatment plan.

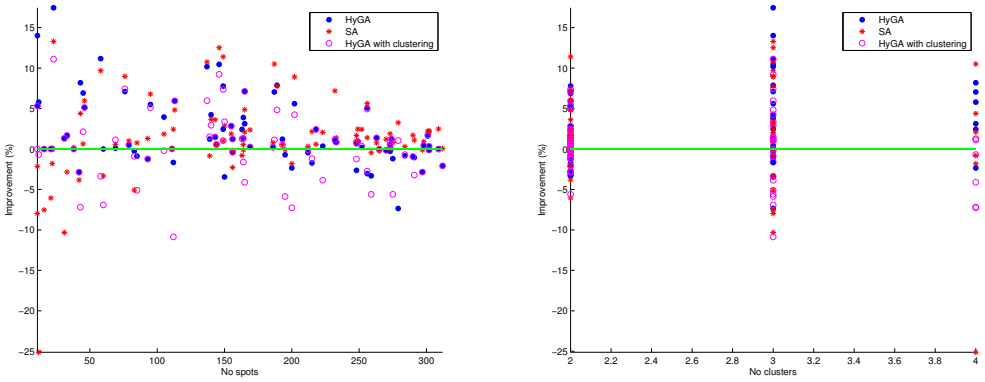

Figure A.9: Path length improvement, TP9. The improvement is shown as a function of the number of irradiation spots (left) and clusters (right) in a treatment plan.

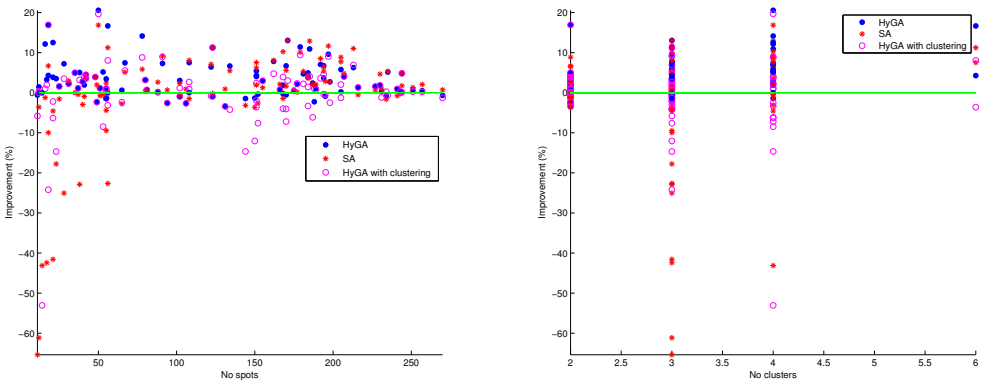

Figure A.10: Path length improvement, TP10. The improvement is shown as a function of the number of irradiation spots (left) and clusters (right) in a treatment plan.

A.2 Clinical Implications

In this section it is shown the number of particles wasted, due to the use of chopper, and the number of particles delivered in each one of treatment plan that were considered for this study. The relative difference value in the tables is between the value obtained with the proposed methods and the value obtained with CNAO's TPS. A negative relative difference value represents the perceptual reduction in the number of particles delivered/wasted with the CNAO's TPS.

Table A.1: Particles delivered ($\mathbf{P_{Delivered}}$) and particles wasted ($\mathbf{P_{wasted}}$) in TP1.

Algorithm	$P_{Delivered}$	Relative difference (%)	$P_{Delivered}$	Relative difference (%)
CNAO's TPS	7.11E+08	-	6.78E+14	-
Simulated Annealing	1.00E+08	-85.9	6.99E+14	3.0
HyGA	4.03E+07	-94.3	7.16E+14	5.5
HyGA with clustering	1.06E+09	49.0	6.68E+14	-1.6

Table A.2: Particles delivered ($\mathbf{P_{Delivered}}$) and particles wasted ($\mathbf{P_{wasted}}$) in TP2.

Algorithm	$P_{Delivered}$	Relative difference (%)	$P_{Delivered}$	Relative difference (%)
CNAO's TPS	1.51E+07	-	1.50E+11	-
Simulated Annealing	1.28E+06	-91.6	1.58E+11	5.2
HyGA	1.64E+06	-89.2	1.60E+11	6.6
HyGA with clustering	1.57E+07	3.9	1.55E+11	3.0

Table A.3: Particles delivered ($\mathbf{P_{Delivered}}$) and particles wasted ($\mathbf{P_{wasted}}$) in TP3.

Algorithm	$P_{Delivered}$	Relative difference (%)	$P_{Delivered}$	Relative difference (%)
CNAO's TPS	1.25E+08	-	1.36E+12	-
Simulated Annealing	6.41E+06	-99.1	1.44E+12	6.5
HyGA	2.33E+06	-99.7	1.39E+12	2.3
HyGA with clustering	1.68E+08	-76.3	1.27E+12	-6.4

Table A.4: Particles delivered ($P_{Delivered}$) and particles wasted (P_{wasted}) in TP4.

Algorithm	$P_{Delivered}$	Relative difference (%)	$P_{Delivered}$	Relative difference (%)
CNAO's TPS	7.50E+07	-	7.54E+11	-
Simulated Annealing	0.00E+00	-100.0	7.81E+11	3.5
HyGA	0.00E+00	-100.0	7.55E+11	0.1
HyGA with clustering	4.63E+07	-93.5	6.91E+11	-8.4

Table A.5: Particles delivered ($P_{Delivered}$) and particles wasted (P_{wasted}) in TP5.

Algorithm	$P_{Delivered}$	Relative difference (%)	$P_{Delivered}$	Relative difference (%)
CNAO's TPS	1.35E+08	-	8.31E+11	-
Simulated Annealing	1.11E+07	-98.4	9.10E+11	9.6
HyGA	4.32E+06	-99.4	8.78E+11	5.7
HyGA with clustering	1.79E+08	-74.8	8.14E+11	-2.1

Table A.6: Particles delivered ($P_{Delivered}$) and particles wasted (P_{wasted}) in TP6.

Algorithm	$P_{Delivered}$	Relative difference (%)	$P_{Delivered}$	Relative difference (%)
CNAO's TPS	5.83E+07	-	3.46E+11	-
Simulated Annealing	7.92E+06	-98.9	3.65E+11	5.5
HyGA	2.46E+06	-99.7	3.45E+11	-0.3
HyGA with clustering	6.68E+07	-90.6	2.99E+11	-13.4

Table A.7: Particles delivered ($P_{Delivered}$) and particles wasted (P_{wasted}) in TP7.

Algorithm	$P_{Delivered}$	Relative difference (%)	$P_{Delivered}$	Relative difference (%)
CNAO's TPS	9.56E+07	-	1.35E+12	-
Simulated Annealing	4.59E+07	-93.5	1.48E+12	9.1
HyGA	2.53E+07	-96.4	1.42E+12	5.0
HyGA with clustering	1.58E+08	-77.8	1.31E+12	-3.0

Table A.8: Particles delivered ($P_{Delivered}$) and particles wasted (P_{wasted}) in TP8.

Algorithm	$P_{Delivered}$	Relative difference (%)	$P_{Delivered}$	Relative difference (%)
CNAO's TPS	1.32E+08	-	4.77E+11	-
Simulated Annealing	7.34E+06	-99.0	5.56E+11	16.6
HyGA	6.27E+06	-99.1	5.29E+11	10.8
HyGA with clustering	1.84E+08	-74.1	4.66E+11	-2.30

Table A.9: Particles delivered ($P_{Delivered}$) and particles wasted (P_{wasted}) in TP9.

Algorithm	$P_{Delivered}$	Relative difference (%)	$P_{Delivered}$	Relative difference (%)
CNAO's TPS	9.16E+06	-	1.07E+12	-
Simulated Annealing	1.94E+06	-99.7	1.10E+12	3.1
HyGA	2.95E+06	-99.6	1.08E+12	1.4
HyGA with clustering	2.17E+07	-96.9	1.07E+12	-0.1

Table A.10: Particles delivered ($\mathbf{P_{Delivered}}$) and particles wasted ($\mathbf{P_{wasted}}$) in TP10.

Algorithm	$\mathbf{P_{Delivered}}$	Relative difference (%)	$\mathbf{P_{Delivered}}$	Relative difference (%)
CNAO's TPS	3.32E+07	-	1.19E+12	-
Simulated Annealing	5.73E+06	-99.2	1.22E+12	2.6
HyGA	5.30E+06	-99.3	1.22E+12	2.0
HyGA with clustering	5.83E+07	-91.8	1.19E+12	-0.3